Journal of Molecular Structure 991 (2011) 186–201

Contents lists available at ScienceDirect

Journal of Molecular Structure

journal homepage: www.elsevier.com/locate/molstruc

Ab initio and *semi-empirical* computational studies on 5-hydroxy-4-methyl-5,6-di-pyridin-2-yl-4,5-dihydro-2H-[1,2,4]triazine-3-thione

Tuncay Karakurt [a,*], Muharrem Dinçer [a], Alaaddin Çukurovalı [b], İbrahim Yılmaz [c]

[a] Department of Physics, Faculty of Arts and Sciences, Ondokuz Mayıs University, 55139 Kurupelit, Samsun, Turkey
[b] Department of Chemistry, Faculty of Science Firat University, 23119 Elazig, Turkey
[c] Department of Chemistry, Faculty of Science Karamanoglu Mehmetbey University, 70100 Karaman, Turkey

ARTICLE INFO

Article history:
Received 4 October 2010
Received in revised form 13 February 2011
Accepted 13 February 2011
Available online 17 February 2011

Keywords:
IR and NMR spectroscopy
Onsager
Ab initio calculations
Electronic structure
NBO analysis

ABSTRACT

The title compound, 5-hydroxy-4-methyl-5,6-di-pyridin-2-yl-4,5-dihydro-2H-[1,2,4]triazine-3-thione ($C_{14}H_{13}N_5OS$), was prepared and characterized by electronic spectroscopy and single-crystal X-ray diffraction (XRD). The compound crystallizes in the triclinic space group P-1 with $a = 9.0126(7)$ Å, $b = 9.0126(7)$ Å, $c = 9.5199(8)$ Å, $\alpha = 85.031(7)^\circ$, $\beta = 77.015(7)^\circ$ and $\gamma = 67.983(6)^\circ$. In addition to the molecular geometry, vibrational frequencies and gauge-including atomic orbital (GIAO) ^1H and ^{13}C NMR chemical shift values of the title compound in the ground state have been calculated using the Hartree–Fock (HF) and density functional theory (DFT) methods with 6-31G(d) basis sets, and compared with the experimental data. The calculated results show that the optimized geometries can well reproduce the crystal structural parameters and the theoretical vibrational frequencies, and ^1H and ^{13}C NMR chemical shift values show good agreement with experimental data. To determine conformational flexibility, the molecular energy profile of the title compound was obtained by semi-empirical (AM1) calculations with respect to the selected torsion angle, which was varied from -180° to $+180^\circ$ in steps of 10°. The energetic behaviour of the title compound in solvent media was examined using the B3LYP method with the 6-31G(d) basis set by applying the Onsager and the Polarizable Continuum Model (PCM). The results obtained with these methods reveal that the PCM method provided more stable structure than Qnsager's method. By using TD-DFT method, electronic absorption spectra of the title compound have been predicted and a good agreement with the TD-DFT method and the experimental one is determined. The predicted non-linear optical properties of the title compound are much greater than ones of urea. In addition, the molecular electrostatic potential (MEP), frontier molecular orbitals (FMO) analysis and thermodynamic properties of the title compound were investigated using theoretical calculations.

1. Introduction

The present study is a continuation of our investigation of the characterization of the hydrogen bonds formed by triazine derivatives in the solid state [1–6]. Triazine and its derivatives, as well as its organic and inorganic complexes or salts, can, via multiple hydrogen bonds, develop supramolecular structures by self-assembly of components which contain complementary arrays of hydrogen-bonding sites [7–12]. 1,2,4-Triazines and the compounds derived from them are found to possess a wide variety of pharmacological activities [13]. Triazine derivatives include herbicides having a broad spectrum of action that kill many species of weeds, and also herbicides with a narrow selectivity [14]. There have been relatively fewer reports of 1,2,4-triazine derivatives and their metal complexes compared to the 1,3,5-analogues, although both compounds are well known for their pharmacological and medicinal properties, including anti-cancer and anti-HIV activities [15]. In the context of nuclear waste reprocessing, several possible chelating agents have been tested in liquid–liquid extraction experiments to separate the trivalent minor actinides from the trivalent lanthanides. Various aza-aromatic bases are among the most extensively studied chelating agents since they have shown unique capabilities to extract americium over europium from acidic solutions into an organic phase. Some metal complexes with aza-aromatic bases containing triazine fragments have recently been reported [16–19].

Here we report the molecular and crystal structure of 5-hydroxy-4-methyl-5,6-di-pyridin-2-yl-4,5-dihydro-2H-[1,2,4]triazine-3-thione ($C_{14}H_{13}N_5OS$) (Fig. 1), determined by single-crystal X-ray diffraction study.

Recent papers in the literature concerning the calculation of NMR chemical shift (c.s.) by quantum-chemistry methods display that geometry optimization is a crucial factor in an accurate

* Corresponding author. Tel.: +90 03623121919/5260; fax: +90 03624576081.
E-mail address: tuncaykarakurt@gmail.com (T. Karakurt).

0022-2860/$ - see front matter © 2011 Elsevier B.V. All rights reserved.
doi:10.1016/j.molstruc.2011.02.025

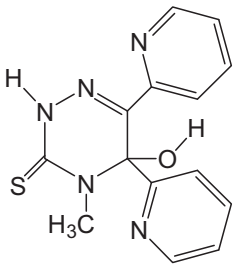

Fig. 1. Chemical structure of the title compound.

determination of computed NMR chemical shift [20–23]. The gauge-including atomic orbital (GIAO) [24,25] method is one of the most common approaches for calculating nuclear magnetic shielding tensors. It has been shown to provide results that are often more accurate than those calculated with other approaches, at the same basis set size [26]. In most cases, in order to take into account correlation effects, post-Hartree–Fock calculations of organic molecules have been performed using: (i) Møller–Plesset perturbation methods, which are very time consuming and hence applicable only to small molecular systems, and (ii) density functional theory (DFT) methods, which usually provide significant results at a relatively low computational cost [27]. In this regard, DFT methods have been preferred in the study of large organic molecules [28], metal complexes [29] and organometallic compounds [30] and for GIAO ^{13}C c.s. calculations [15] in all those cases in which the electron correlation contributions were not negligible. In this study, the geometrical parameters, fundamental frequencies and GIAO ^{1}H and ^{13}C NMR chemical shifts of the title compound in the ground state have been calculated by using the HF and DFT (B3LYP) methods with 6-31G(d) basis set. A comparison of the experimental and theoretical spectra can be very useful in making correct assignments and understanding the basic chemical shift-molecular structure relationship. And so, these calculations are valuable for providing insight into molecular analysis.

2. Experimental and computational methods

All chemicals were of reagent grade and used as commercially purchased without further purification. IR spectra of the compound were recorded in the range of 400–4000 cm^{-1} with a Mattson 1000 FT-IR spectrometer using KBr pellets. The ^{1}H and ^{13}C NMR spectra were recorded on a Varian-Mercury 400 MHz spectrometer using TMS as an internal standard and DMSO-d_6 as solvent. Melting point was determined by Gallenkamp melting point apparatus and is uncorrected. Electronic absorption spectra were measured on a Unicam UV–vis spectrophotometer in ethanol (Scheme 1).

The synthesis of the title compound was simply carried out in the following reaction in Fig. 2. A solution of 10 mmol of 2-hydroxy-1,2-di-pyridin-2-yl-ethanone (pyridoin) and 20 mmol of 4-methyl thiosemicarbazide in 50 mL absolute ethanol was refluxed for 7 h in the presence of 0.005 g *p*-TsOH as catalyst, with continuous stirring and monitoring the course of the reaction by IR spectroscopy. When cooling to room temperature, target product was precipitated with the slow addition of water; filtered, washed with copious cold ethanol and dried in air. The shiny crystals of substance, suitable for X-ray analysis were obtained by slow evaporation from their ethanol solutions, Yield: 1.64 g, 52%; mp 202 °C; FTIR (KBr, cm^{-1}): 3185 (–OH), 3133 (–NH–), 2947 (aliphatics), 1529 (thioamide I), 1292 (thioamide II), 1074 (thioamide III), 612 (thioamide IV); ^{1}H NMR (400 MHz, DMSO-d_6): δ 2.91 (s, 3H, –CH_3), 7.15–7.18 (ddd, 1H, J_1 = 7.41 Hz, J_2 = 4.94 Hz, J_3 = 1.10 Hz), 7.23–7.27 (ddd, 1H, J_1 = 6.69 Hz, J_2 = 4.74 Hz, J_3 = 1.10 Hz), 7.68–7.97 (m, 4H, aromatics), 8.04 (s, 1H, –NH–, D_2O exchangeable), 8.17–8.19 (ddd, 1H, J_1 = could not be detected, J_2 = 4.79 Hz, J_3 = ~1 Hz), 8.37–8.40 (ddd, 1H, J_1 = could not be detected, J_2 = 4.39 Hz, J_3 = ~1 Hz), 12.00 (s, 1H, –OH, D_2O exchangeable); ^{13}C NMR (400 MHz, DMSO-d_6): δ 171.22, 160.28, 153.42, 149.34, 148.43, 143.48, 137.32, 136.96, 124.05, 123.78, 122.38, 122.28, 82.79, 33.71. Anal. calcd. for $C_{14}H_{13}N_5OS$: C, 56.17; H, 4.38; N, 23.40; S, 10.71. Found: C, 55.90; H, 4.41; N, 22.97; S, 10.48 (Scheme 2).

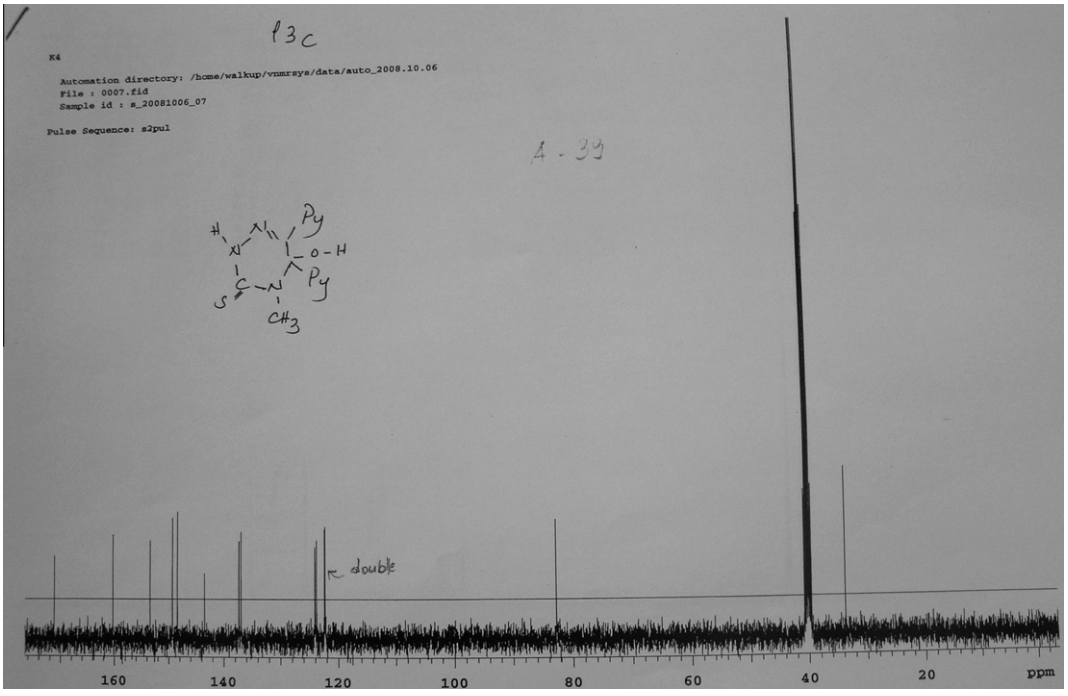

Scheme 1.

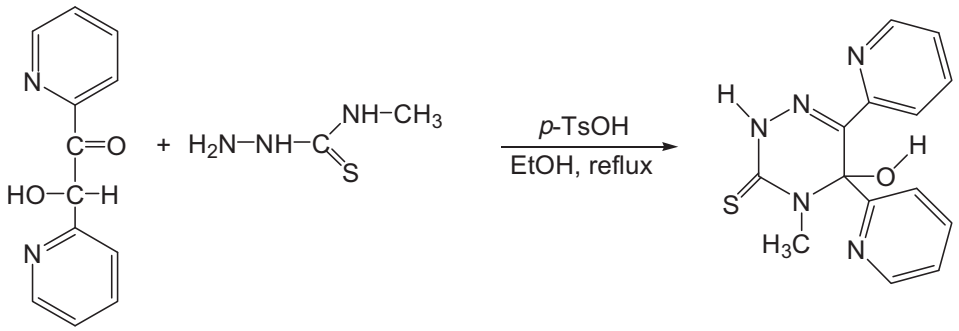

Fig. 2. Synthetic route for the synthesis of the target compound.

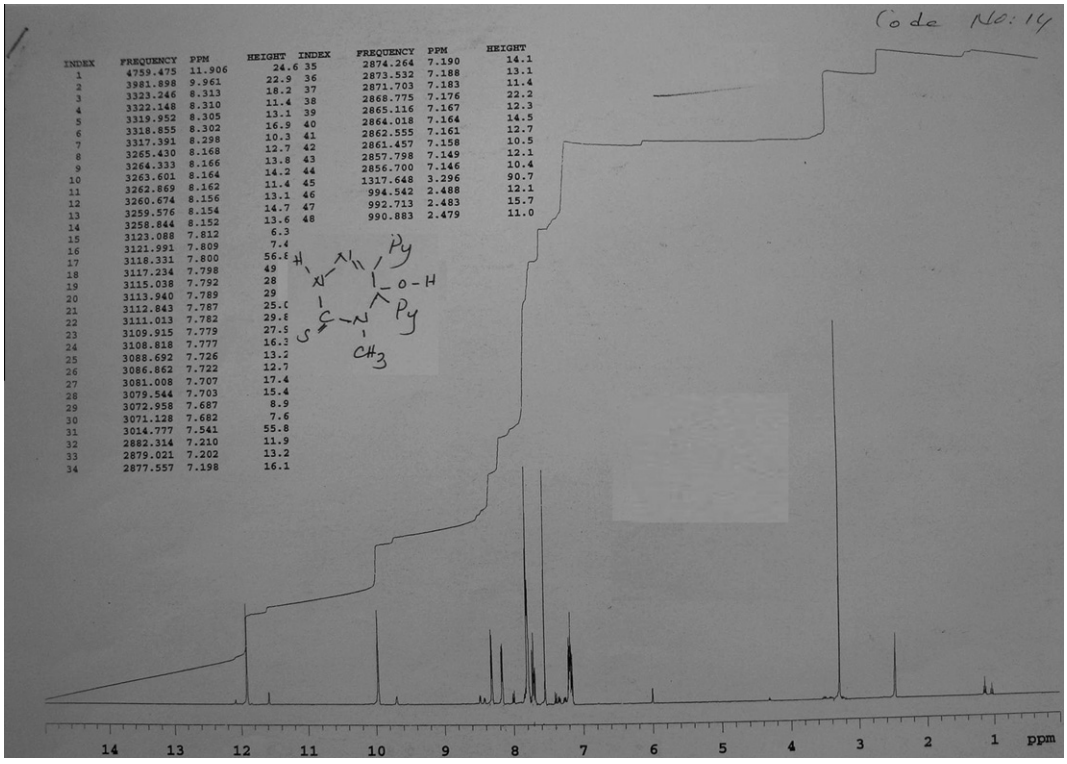

Scheme 2.

2.1. X-ray crystallography general

A suitable sample of size 0.650 × 0.427 × 0.210 mm was selected for the crystallographic study. All diffraction measurements were performed at room temperature (296 K) using graphite monochromated Mo Kα (λ = 0.71073 Å) radiation and an STOE IPDS 2 diffractometer. A total of 28334 reflections with [2.20° < θ < 27.56°] were collected in the rotation mode and cell parameters were determined by using X-AREA software [31]. Absorption correction (μ = 0.24 mm^{-1}) was achieved by the integration method via X-RED software [31]. The structure was solved by direct methods using SHELXS-97 [32]. The refinement was carried out by full-matrix least-squares method on the positional and anisotropic temperature parameters of the non-hydrogen atoms, or equivalently corresponding to 190 crystallographic parameters. All non-hydrogen atom parameters were refined anisotropically and all H atom parameters were freely refined. H atoms were added at calculated positions and refined using a riding model with $U_{iso}(H) = xU_{eq}$ (*parent atom*), where x = 1.5 for methyl and 1.2 for others. The U_{iso} values for H atoms are in the range 0.054–0.128. Non-hydrogen atomic coordinates and equivalent isotropic thermal parameters are listed in Table 1.

The structure was refined to R = 0.0488 for observed reflections and to R = 0.0543 for all data. The maximum peaks and deepest hole observed in the final Δp map were 0.347 and −0.350 e Å^{-3}, respectively. The scattering factors were taken from SHELXL-97 [32].

2.2. Computational details

The molecular structure of the title compound in the ground state (*in vacuo*) was optimized using Hartree–Fock (HF) and DFT(B3LYP) [33,34] with the 6-31G(d) [35] basis set. For modelling, the initial guess of the title compound was first obtained from the X-ray coordinates. Then, vibrational frequencies for the optimized molecular structures of the title compound were calculated using these methods and then scaled by 0.8929 and 0.9613 [36], respectively. The geometry of the title compound, together with that of

Table 1
Atomic coordinates and equivalent isotropic displacement parameters (Å^2) of the non-hydrogen atoms for the title compound.

Atom	x	y	z	U_{eq}
O1	0.41244	0.28456	−0.42700	0.06093
N1	0.60410	0.25749	−0.12596	0.04019
N2	0.70094	0.08011	−0.53471	0.06964
N3	0.29123	0.25306	−0.19196	0.04407
N4	0.38944	0.00072	−0.09784	0.04495
N5	0.52491	−0.05340	−0.20476	0.04210
S1	0.09822	0.18011	0.03784	0.06504
C1	0.53613	0.32144	−0.23836	0.03954
C2	0.54247	0.46317	−0.30179	0.06369
C3	0.62295	0.54197	−0.24829	0.06939
C4	0.69577	0.47649	−0.13514	0.05611
C5	0.68343	0.33523	−0.07728	0.04967
C6	0.44803	0.22718	−0.29198	0.04104
C7	0.26752	0.14693	−0.09113	0.04136
C8	0.55313	0.04907	−0.29800	0.03973
C9	0.70003	−0.01201	−0.41581	0.05067
C10	0.82770	−0.15483	−0.40232	0.06472
C11	0.95882	−0.20396	−0.51829	0.09306
C12	0.96034	−0.11171	−0.64035	0.10632
C13	0.83071	0.02768	−0.64416	0.09586
C14	0.16324	0.41209	−0.19701	0.06512

Note. U_{eq} is defined as one third of the trace of the orthogonalized U_{ij} tensor.

Table 2
Crystallographic data for title compound.

Formula	$C_{14}H_{13}N_5OS$
Formula weight	299.35
Temperature (K)	293 K
Wavelength (Å)	Mo Kα, 0,71073
Crystal system	Triclinic
Space group	P-1
Unit cell	
a (Å)	9.0126(7)
b (Å)	8.9676(7)
c (Å)	9.5199(8)
α (°)	85.031(7)^0
β (°)	77.015(7)^0
γ (°)	67.983(6)^0
V (Å^3)	695.05(10)
Z	2
D_{calc} (g/cm^3)	1.43
F (0 0 0)	312
h, k, l Range	$-11 \leqslant h \leqslant 11$
	$-11 \leqslant k \leqslant 11$
	$-12 \leqslant l \leqslant 12$
Reflections collected	11643
Independent reflections	3199
R_{int}	0.0462
Reflections observed [$I \geqslant 2\sigma(I)$]	2641
Data/restraints/parameters	3199/0/190
R [$I > 2\sigma(I)$]	0.0448
R_w [$I > 2\sigma(I)$]	0.1272
Goodness-of-fit on Indicator	1.026
Structure determination	Shelxs-97
Refinement	Full matrix
$(\Delta\sigma)_{max}$, $(\Delta\sigma_{min})$ (e/Å^3)	0.347, −0.350

tetramethylsilane (TMS), is fully optimized. ^{1}H and ^{13}C NMR chemical shifts were calculated within the GIAO approach [37,25] applying the same methods and basis set as used for geometry optimisation. The ^{1}H and ^{13}C NMR chemical shifts were converted to the TMS scale by subtracting the calculated absolute chemical shielding of TMS ($\delta = \Sigma_0 - \Sigma$, where δ is the chemical shift, Σ is the absolute shielding and Σ_0 is the absolute shielding of TMS), with values of 32.52 and 199.79 ppm for HF/6-31G(d) and 32.10 and 189.40 ppm for B3LYP/6-31G(d), respectively. All calculations were performed using the Gauss-View Molecular Visualization program [38,39] and Gaussian 03 program package [40] on a personal computer without specifying any symmetry for the title molecule. The effect of solvent on the theoretical NMR parameters was included using the default model Integral-Equation-Formalism Polarizable Continuum Model (IEF-PCM) [41] provided by Gaussian 03. Dimethylsulfoxide (DMSO), with a dielectric constant (ε) of 46.7, was used as solvent. A preliminary search of low-energy structures was carried out with the AM1 computations. Conformational energies were calculated as a one-dimensional scan by varying the φ_1(N2–C9–C8–N5) and φ_2(C2–Cl–C6–C8) dihedral angles from

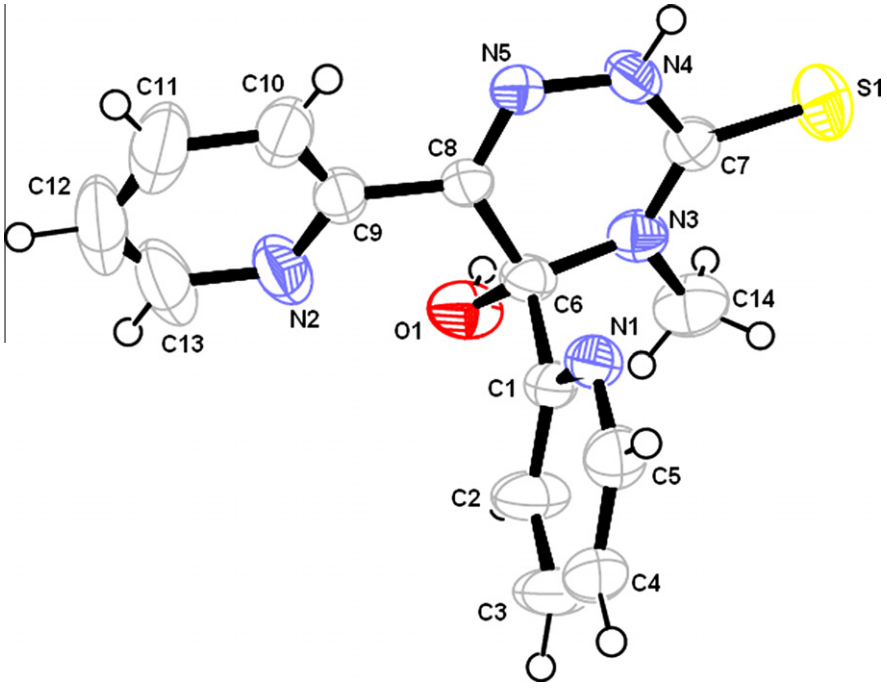

Fig. 3. An ORTEP view of the title compound with the atomic numbering scheme. Displacement ellipsoids are shown at the 20% probability level.

−180° to +180° in steps of 10°, and the molecular energy profile was obtained. In order to investigate the total energy and dipole moment behaviour of the title compound in solvent media, we also carried out optimization calculations in five solvents [ε = 4.90, chloroform ($CHC1_3$); ε = 10.36, dichloroethane (CH_2ClCH_2Cl); ε = 24.55, ethanol (C_2H_5OH); ε = 46.7, DMSO; ε = 78.39, water (H_2O)] at the B3LYP/6-31G(d) level using the Onsager [42] and Polarizable Continuum Model (PCM) [43–46] methods. The electronic absorption spectra were calculated using the time-dependent density functional theory (TD-DFT) method [47–50]. In addition, the electronic absorption spectra were calculated in ethanol solution with the PCM method. To investigate the reactive sites of the title compound, the MEP were evaluated using B3LYP/6-31G(d) method. MEP, $V(\mathbf{r})$, at a given point $\mathbf{r}(x, y, z)$ in the vicinity of a molecule, is defined in terms of the interaction energy between the electrical charge generated from the molecule's electrons and nuclei and a positive test charge (a proton) located at $\mathbf{r}$. For the system studied the $V(\mathbf{r})$ values were calculated as described previously using the equation [51],

$$V(r) = \sum_A \frac{Z_A}{|R_A - r|} - \int \frac{\rho(r')}{|r' - r|} dr'$$

where Z_A is the charge of nucleus A, located at R_a, $p(r')$ is the electronic density function of the molecule, and r' is the dummy integration variable. The mean linear polarizability and mean first hyperpolarizability properties of the title compound were obtained by molecular polarizabilities basing on theoretical calculations. In addition frontier molecular orbitals (FMO) were performed with B3LYP/6-31G(d) the optimized structure.

3. Results and discussion

3.1. Geometrical structure

In order to expand the understanding of the solid-state physical–organic chemistry of compounds containing multiple and different hydrogen-bonding systems, we have studied the solid-state structure of 5-hydroxy-4-methyl-5,6-di-pyridin-2-yl-4,5-dihydro-2H-[1,2,4]triazine-3-thione ($C_{14}H_{13}N_5OS$). The title compound. An Ortep-3 [52] view of which is show in Fig. 3, crystallizes in the triclinic space group P-1 with four molecules in the unit cell. The data collection Conditions and parameters of refinement process are listed in Table 2.

Table 3
Hydrogen bonding geometry (Å, °) for the title compound.

D–H···A	D–H	H···A	D···A	D–H···A
N4–H4A···N1^{i}	0.860	2.151	3.001	169.72
Ol–H1···Cgl^{ii}	0.820	2.85	3.575	149

Symmetry codes: (i) $-x + 1, -y, -z$; (ii) $1 - x, -y, 1 - z$.
Cgl: the centroid of the N2/C9–C13 ring.

The title molecule can be described as being built from planar fragments, *viz.* triazine ring *A*(C8/C6/N3/C14/C7/S1/N4/N5) linking two pyridine rings *B*(N2/C9–C13) and *C*(N1/C1–C5). The triazine ring is essentially planar, the largest deviation from the mean plane being 0.112(2) Å for atom C6. 1,2,4 triazine ring of (Fig. 3) is significantly distorted from the ideal hexagonal form, with the internal C8–C6–N3 angle significantly smaller than 120°. This is a result of the steric effect of a lone-pair electron, predicted by the valence-shell electron-pair repulsion theory [53,54]. This is undoubtedly due to the direct bond between the two N atoms (N5–N4), which partially reduces the steric effect of the lone-pair electrons. Additionally, the steric effect of the lone-pair electrons on the N4 and N5 ring atoms is reduced due to hydrogen bonds, in which both ring N atoms are involved as acceptors (Fig. 4).

The dihedral angles between the triazine plane *A*(C8/C6/N3/C14/C7/S1/N4/N5), the pyridin rings *B*(N2/C17–C20) and *C*(N1/C1–C5) are 19.34(12)° (*AIB*), 85.00(9)° (*AIC*), 87.98(12)° (*B/C*). The triazine ring is planar and exists in the thione form; the C=S bond length of 1.6749(16) is slightly longer than the pure double-bond distance (1.61 Å; [55]). The N–N [1.3584(18) Å], C–N [mean value 1.358(2) Å] and C=N [1.276(2) Å] bond distances are intermediate between the expected single (1.45 and 1.47 Å, respectively) and double (1.20 and 1.27 Å, respectively) bond distances. The bond angles and bond lengths (Table 4) in the triazine ring are within the normal ranges. There are one N–H···N and one X–H···Cg (π-ring) (edge-to-face) intermolecular interactions, details of which are given in Table 3. Amino atom N4 in the molecule at (x, y, z) acts as hydrogen-bond donor, *via* atom H4A, to ring atom N1 in the molecule at $(-x + 1, -y, -z)$ and characterized by an $R_2^2(14)$ motif [56] (Fig. 4). The atom O1 at (x, y, z) forms a O–H···Cg (π-ring) contact, this time *via* atom H1, with the centroid of the N2/C9-C13 ring [*fractional centroid coordinates:* 0.82973(13), −0.06245(16), 0.47406(11)] of the molecule at $(1 - x, -y, 1 - z)$.

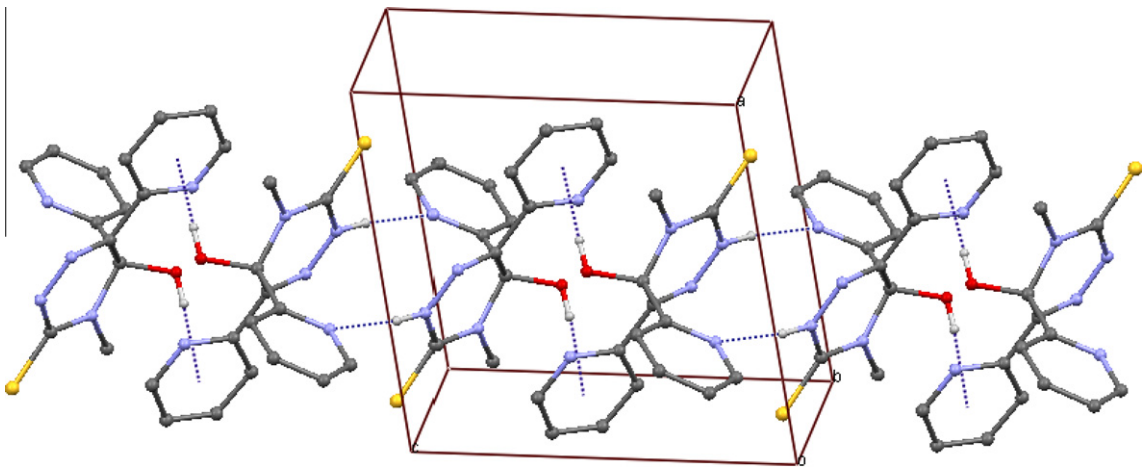

Fig. 4. Part of the crystal structure of the title molecule, showing the formation of a chain of centrosymmetric $R_2^2(14)$ dimers. For clarity, only H atoms involved in hydrogen bonding have been included. For the sake of clarity, H atoms not involved in the motifs shown have been omitted.

Table 4
Selected optimized and experimental geometric parameters in the ground state.

Parameters	Experimental	Calculated	
		HF 6-31G(d)	B3LYP 6-31G(d)
C6–O1	1.4024(19)	1.388	1.409
C5–N1	1.338(2)	1.318	1.336
C1–N1	1.332(2)	1.321	1.34
C1–C6	1.538(2)	1.538	1.545
C6–N3	1.465(2)	1.459	1.478
C14–N3	1.465(2)	1.464	1.466
S1–C7	1.6749(16)	1.685	1.68
N4–N5	1.3584(18)	1.341	1.424
N4–C7	1.354(2)	1.348	1.379
C8–N5	1.276(2)	1.254	1.289
C8–C9	1.485(2)	1.493	1.48
N2–C9	1.342(3)	1.323	1.349
N2–C13	1.343(3)	1.323	1.338
C9–C10	1.383(3)	1.392	1.406
RMSE[a]		0.0077	0.0191
Max. difference[a]		0.431	0.191
Bond angles (°)			
C2–C1–N1	122.44(15)	122.9	123.15
C1–C2–C3	119.07(18)	118.11	118.33
O1–C6–C8	111.22(13)	110.65	111.15
O1–C6–C1	110.68(12)	111.81	111.61
N3–C6–C8	109.62(12)	109.79	109.32
N3–C6–C1	108.93(13)	108.96	108.72
C6–N3–C14	116.12(14)	116.48	116.61
C7–N3–C14	120.26(15)	119.35	119.04
N3–C7–N4	116.37(14)	116.48	115.6
N3–C7–S1	124.93(12)	125.21	125.79
N4–C7–S1	118.69(12)	118.31	118.59
C8–N5–N4	117.36(13)	118.99	118.15
C9–N2–C13	117.57(11)	119.19	118.97
C9–C10–C11	117.72(12)	118.37	118.89
RMSE[a]		0.8836	0.8678
Max. difference[a]		16.25	17.07
Dihedral angles (°)			
N1–C5–C4–C3	0.20(3)	−0.1	−0.1
C4–C5–N1–C1	1.00(3)	−0.01	0.07
C7–N4–N5–C8	10.50(2)	6.84	10.48
N5–N4–C7–N3	−7.20(2)	−3.87	−6.12
N5–N4–C7–S1	171.19(13)	175.59	172.43
N4–N5–C8–C9	−178.99(14)	178.56	179.1
N4–N5–C8–C6	2.50(2)	−0.63	0.97
C11–C10–C9–N2	−1.30(3)	−0.41	0.01
N5–C8–C9–N2	159.63(16)	161.55	167.41
C6–C8–C9–N2	−21.80(2)	−19.22	−14.38
N5–C8–C9–C10	−20.70(2)	−18.67	−12.76
C7–N3–C6–O1	139.90(15)	129.56	138.29
C14–N3–C6–01	−46.76(19)	−55.34	−51.39
N5–C8–C6–O1	−133.74(17)	−123.82	−130.87
N1–C1–C6–O1	−167.29(14)	−173.21	−173.19
C2–C1–C6–O1	13.40(2)	7.85	7.99
N1–C1–C6–N3	75.51(17)	69.64	69.78
C2–C1–C6–C8	136.30(18)	130.73	131.55

3.2. Theoretical structure

The atomic numbering scheme the theoretical geometric structure of the title compound are shown in Fig. 5.

Selected geometric parameters obtained experimentally and those calculated theoretically using HF and B3LYP with the 6-31G(d) basis set are listed in Table 4. It is well known that DFT-optimized bond lengths are usually longer and more accurate than HF, due to the inclusion of electron correlation. However, according to our calculations, the HF method correlates well for the bond length compared with the other method (Table 4). Although the largest difference between experimental and calculated bond lengths is about 0.431 Å for HF and 0.191 Å for B3LYP, the root mean square error (RMSE) is found to be about 0.0077 Å for HF and 0,0191 Å for B3LYP, indicating that the bond lengths obtained by the HF method show the strongest correlation with the experimental values. However, this time, both the largest difference and the root mean square error for the bond angles obtained by the B3LYP method are smaller than those determined by HF. When the X-ray structure of the title compound is compared with its optimized counterparts (see Fig. 6), slight conformational discrepancies are observed The dihedral angle between the triazine and pyridin rings is calculated at 161.55° (*A*/*B*) and 69.65° (*A*/*C*) for HF and at 167.41° (*A*/*B*), 69.78° (*A*/*C*) for B3LYP. A logical method for globally comparing the structures obtained with the theoretical calculations is by superimposing the molecular skeleton with that obtained from X-ray diffraction, giving a RMSE of 0.160 Å for HF/6-31G(d) and 0.106 Å for B3LYP/6-31G(d) calculations (Fig. 6). Consequently, the B3LYP method correlates well for the geometrical parameters when compared with HF.

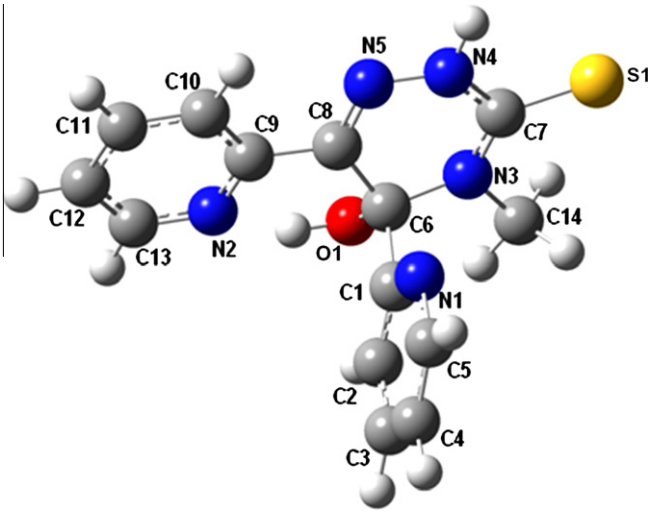

Fig. 5. The theoretical geometric structure of the title compound.

3.3. Conformational analysis

Based on HF/6-31G(d) and B3LYP/6-31G(d) optimized geometries, the total energy of the title compound has been calculated by these methods, which are −1282.3177 and −1288.4634, a.u., respectively, while the dipole moment has been calculated as 9.5104 and 7.6721 Debye. In order to define the preferential positions of pyridine with respect to triazine ring, a preliminary search of low-energy structures was performed using AM1 computation as a function of the selected degrees of torsional freedom, φ_1(N2–C9–C8–N5) and φ_2(C2–Cl–C6–C8). The respective values of the selected degrees torsional freedom, φ_1(N2–C9–C8–N5) and φ_2(C2–Cl–C6–C8), are 159.63(16)° and 136.30(18)°, respectively in X-ray structure, whereas the corresponding values in optimized geometries 161.55° and 130.73°, respectively for HF/6-31G(d) and 167.41° and 131.55°, respectively for B3LYP/6-31G(d).

The molecular 1-D energy profiles with respect to rotations about the selected torsion angles are presented in Fig. 7. According to the results, the low-energy domains for φ_1(N2–C9–C8–N5) are located at −150°, −100° and 110° with energies of 112.952, 111.069 and 109.814 kcal mol^{-1}, respectively, while they are located at −60°, −20°, and 100° having energy of 112.952, 111.697 and 112.324 kcal mol^{-1}, respectively, for φ_2(C2–Cl–C6–C8). Energy difference between the most favorable and unfavorable conformers, which arises from rotational potential barrier calculated with respect to the two selected torsion angles, is calculated as 3.884 kcal mol^{-1} for φ_1(N2–C9–C8–N5) and as 5.974 kcal mol^{-1}

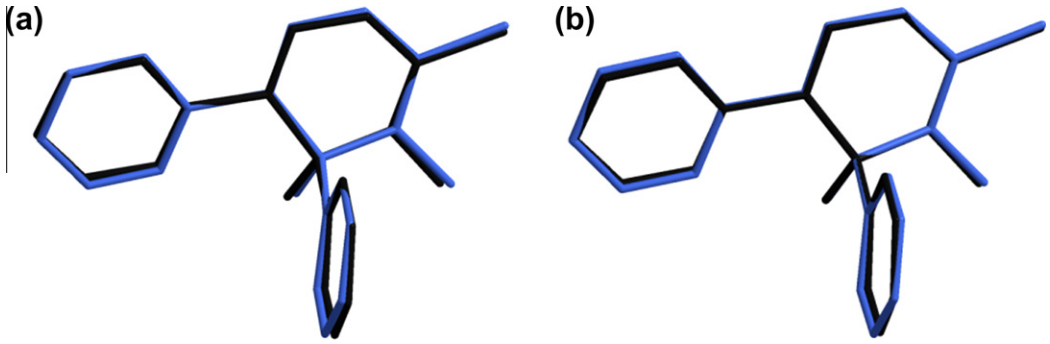

Fig. 6. Atom-by-atom superimposition of the structures calculated (blue) [*a* = HF; *b* = BLYP with 6-31G(d)] over the X-ray structure (black) for the title compound. Hydrogen atoms omitted for clarity. (For interpretation of the references to colour in this figure legend, the reader is referred to the web version of this article.)

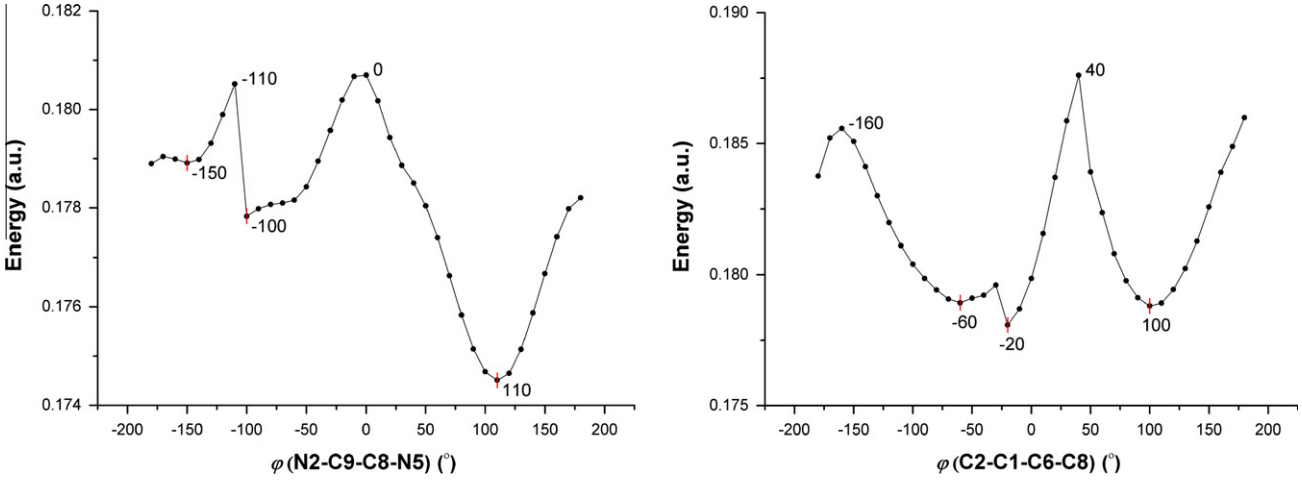

Fig. 7. Molecular energy profile against the selected torsional degrees of freedom using AM1.

for φ_2(C2–Cl–C6–C8), when both selected degrees of torsional freedom are considered.

3.4. IR spectroscopy

The IR spectra were measured with Mattson 1000 Fourier transform (FT)-IR spectrophotometer using KBr pellets and shown in Fig. 8a. In order to obtain the spectroscopic signature of the selected compounds, we performed a frequency calculation analysis. The harmonic-vibrational frequencies are calculated for the title compounds by HF/6-31G(d) and B3LYP/6-31G(d) methods. Table 5 present the calculated and experimental fundamental vibrational frequencies, IR intensities of the title compound. In addition, it is noted that the vibrational frequencies over the region 4000–400 cm^{-1} are listed in Table 5. The theoretically FT-IR spectra of title compound by HF and B3LYP methods are shown in Fig. 8b. Any discrepancy noted between the observed and the calculated frequencies may be due to the two facts: one is that the experimental results belong to solid phase and theoretical calculations belong to gaseous phase; the other is that the calculations have been actually done on a single molecule contrary to the experimental values recorded in the presence of intermolecular interactions.

The molecule of title compound consists of 34 atoms. The 96 normal modes of vibration of title compound, which span in the irreducible representations as 96A under the C1 point group symmetry, have been assigned according to the detailed motion of the individual atoms.

3.4.1. C–H vibrations

The heteroaromatic structure shows the presence of C–H stretching vibration in the region 3100–3000 cm^{-1}, which is the characteristic region for the ready identification of C–H stretching vibration [57,58]. In this region, the bands are not affected appreciably by the nature of the substituent. As the title compound consists of two pyridine groups which are bridged by triazine ring has two adjacent and one C–C isolated moieties in each of pyridine ring. The six expected C–H stretching vibrations correspond to stretching modes of C2–H, C3–H, C4–H, C10–H, C11–H and C12–H units. Hence in our present work, the FT-IR band observed at 3068 and 3030 cm^{-1} are assigned to C–H stretching vibration. The calculated bands at 3067–3058 cm^{-1} for HF/6-31G(d) and 3121–3110 cm^{-1} for B3LYP/6-31G(d). The aromatic C–H in-plane bending vibration occurs in the region 1300–1000 cm^{-1}, the bands are sharp but have weak-to-medium intensity. The C–H in-plane bending vibration computed at 1294, 1198, 1185 and 1012 cm^{-1} for HF/6-31G(d) and at 1255, 1201, 1068 and 1002 for B3LYP/6-31G(d) methods shows excellent agreement with FT-IR bands at 1228, 1190 and 1027 cm^{-1}. The bands observed at 830 and 687 cm^{-1} in FT-IR are assigned to C–H out-of-plane bending vibration for title compound. This also shows good agreement with theoretically scaled harmonic wavenumber values at 965 and 719 cm^{-1} for HF/6-31G(d) and at 914 and 695 cm^{-1} for B3LYP / 6-31G(d).

3.4.2. C–C vibrations

The aromatic ring vibrational modes of title compound have been analyzed based on the vibrational spectra of previously pub-

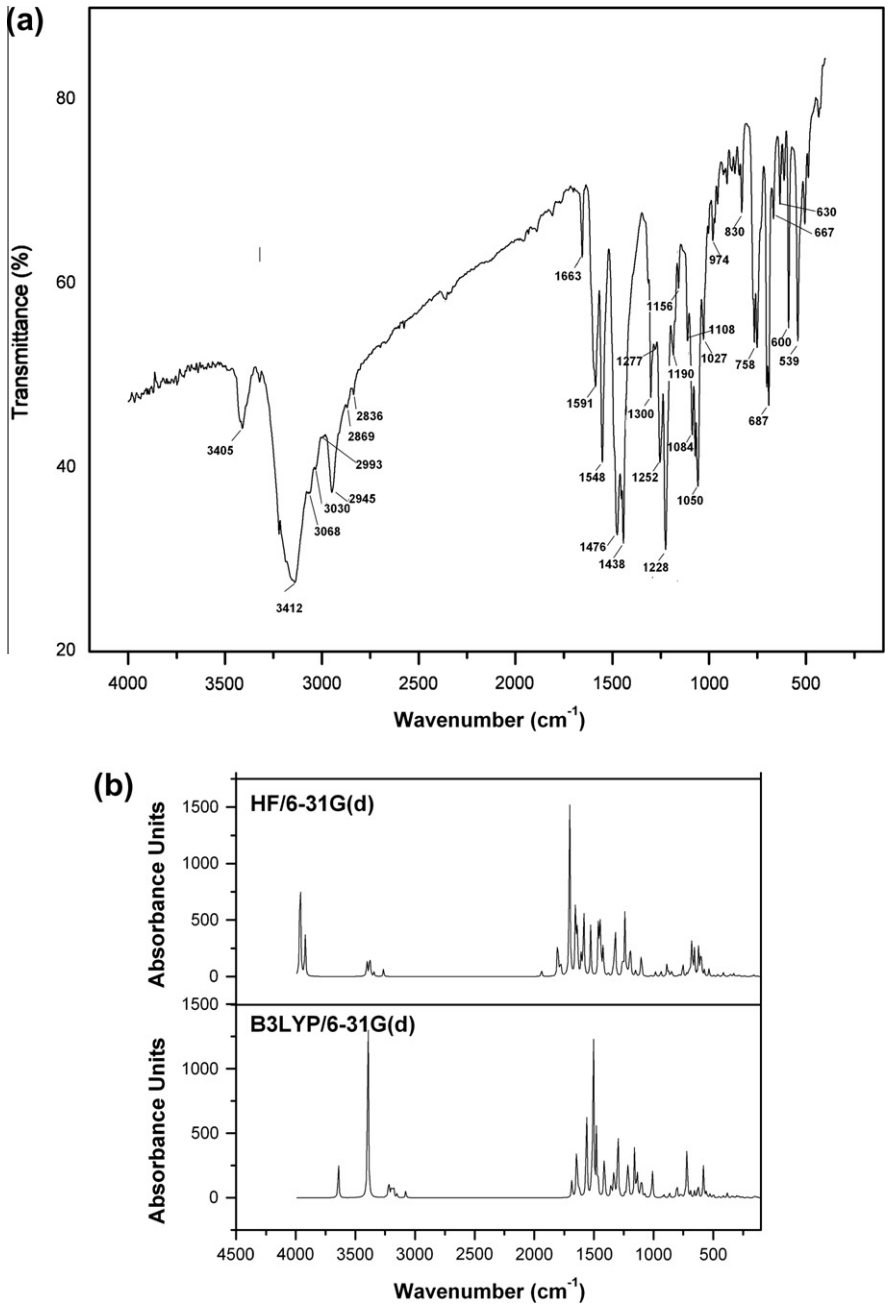

Fig. 8. (a) Experimental (b) Comparison theoretical FT-IR spectrum.

lished vibrations of the benzene molecule are helpful in the identification of the phenyl ring modes [59,60]. Both the phenyl rings are m- and p-substituted derivatives. The ring stretching vibrations are very prominent, as the double bond is in conjugation with the ring, in the vibrational spectra of benzene and its derivatives [61]. The ring carbon–carbon stretching vibrations occur in the region 1625–1430 cm^{-1}. In general, the bands are of variable intensity and are observed at 1625–1590, 1590–1575, 1540–1470, 1465–1430 and 1380–1280 cm^{-1} from the wavenumber ranges given by Varsanyi [62] for the five bands in the region. In the present work, the wavenumbers observed in the FT-IR spectrum at 1600, 1509, 1427 and 1371 cm^{-1} have been assigned to C=C stretching vibrations. The theoretically computed values at 1602, 1595, 1585, 1573, 1500, 1494, 1420, 1408 and 1385 cm^{-1} show an excellent agreement with experimental data. These modes are mixed mode with the contribution of C–H in-plane bending vibration in this region. The in-plane deformation vibrations are at higher wavenumbers than the out-of-plane vibrations. Shimanouchi et al. [63] gave the wavenumber data for these vibrations for five different benzene derivatives as a result of normal coordinate analysis. The bands observed at 630 cm^{-1} in FT-IR are assigned to C–C–C deformation vibrations of the pyridine rings. The theoretically computed values at 623 cm^{-1} for HF/6-31G(d) and at 645 cm^{-1} for the B3LYP/6-31G(d) methods are in excellent agreement with experimental data.

3.4.3. O–H vibrations

The O–H group gives rise to three vibrations (stretching, in-plane bending and out-of-plane bending vibrations). The O–H group vibrations are likely to be the most sensitive to the environment, so they show pronounced shifts in the spectra of the hydrogen bonded species. The hydroxyl stretching vibrations are

Table 5
Comparison of the observed and calculated vibrational spectra of title compound.

Assignments	FT-IR (cm^{-1}) with KBr [15]	Scaled frequencies (6-31G(d)) (cm^{-1}) and intensity (I_{IR}, km/mol)) and relative intensity (I, km/mol)			
		HF	I_{IR}	B3LYP	I_{IR}
ν N–H str.	3185	3390	464	3502	104
ν O–H str.	3133	3200	82	3263	16
ν ring C–H str.	3068	3067	1	3121	2
ν ring C–H str.	3030	3058	2	3113	2
ν ring C–H str.	–	3039	24	3098	21
ν_{as} CH_3 str.	2993	2985	12	3028	10
ν CH_3 str.	–	2914	19	2959	73
ν ring C–H str.	2945	2876	41	2921	55
ν_{as} ring C–H str. + ν CH_3 str.	2869	2798	74	2822	17
ν_{as} ring C–H str.	2836	2911	258	2899	14
ν N=C str.	1663	1702	101	1700	21
ν C–C aromatic str.	1591	1643	75	1510	33
ν N–N str.	1548	1490	90	1540	59
ν N–C str.	1476	1458	83	1420	46
ν C–C aromatic str.	1438	1400	27	1410	13
ρ C–H aromatic	–	1294	144	1255	88
ν N–N str. + ν N–C str	1300	1291	23	1215	38
ν C–O str.	1277	1240	33	1211	13
ρ O–H bending + ν C–C aromatic str.	1252	1222	30	1200	11
ρ O–H bending + γ C–H aromatic.	1228	1198	62	1201	37
θ ring + β N–H bending + γ C–H aromatic.	1190	1185	19	1168	187
ω CH_3 wag.	1156	1155	229	1160	33
θ	1108	1100	48	1102	12
θ	1084	1099	131	1099	5
α CH_3 scis.	1050	1050	210	1023	3
γ C–H aromatic.	1027	1012	196	1002	15
ν C=S str.	974	979	201	925	5
β out-of-plane bending CH	830	965	124	914	3
ω ring CH wag.	758	867	111	793	4
β out-of-plane bending CH + β O–H bending	687	719	143	695	27
O–H bending	–	602	77	693	7
γ CH_3 roc.	667	630	271	665	18
β C–C–C aromatic str.	630	623	102	645	116
ρ C–C=N aromatic str.	600	567	91	585	116
ρ C–C–C aromatic str.	539	547	99	525	

ν: stretching, ν_{as}: asymmetric stretching, δ: bending, ρ: in-plane bending, β: out-of-plane bending, γ: rocking, ω: wagging, θ: ring breathing.

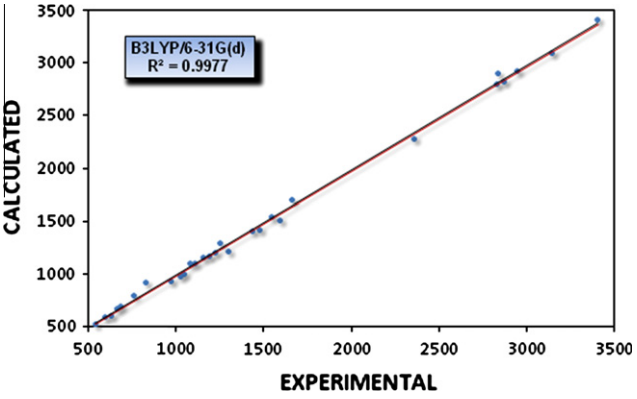

Fig. 9. Correlation graphics of calculated and experimental frequencies.

Table 6
Theoretical and experimental ^{13}C and ^{1}H isotropic chemical shifts (with respect to TMS, all values in ppm).

Atom	Experimental(ppm) (DMSO-d_6)	Calculated(ppm)	
		HF 6-31G(d)	B3LYP 6-31G(d)
C1	160.28	161.07	155.28
C2	122.38	118.80	115.34
C3	137.32	140.76	130.20
C4	122.28	121.37	117.86
C5	143.48	151.53	143.17
C6	82.79	76.26	83.76
C7	171.22	176.73	166.3
C8	153.42	147.86	136.26
C9	149.34	155.34	147.16
C10	123.78	120.16	116.53
C11	136.96	142.13	131.41
C12	124.05	121.96	118.29
C13	148.83	148.91	140.52
C14	33.71	30.42	31.75
H (CH_3)	2.91	2.89*	2.83*
H (CH aromatik)	7.15–8.40	8.31*	7.91*
H (NH)	8.04	8.96	8.70
H (OH)	12.00	8.57	7.66

* Average.

generally [64] observed in the region around 3500 cm^{-1}. In the case of the un-substituted phenols it has been shown that the frequency of O–H stretching vibration in the gas phase is 3657 cm^{-1} [65]. Similarly in our case a very strong FT-IR band at 3133 cm^{-1} is assigned to O–H stretching vibrations. A comparison of this band with that of the computed by B3LYP/6-31G(d) method at 3263 cm^{-1} show positive deviation of ~130 cm^{-1}, this may bedue to the presence of strong intermolecular hydrogen bonding.

The O–H in-plane bending vibration in phenols, in general lies in the region 1150–1250 cm^{-1} and is not much affected due to hydrogen bonding unlike to stretching and out-of-plane bending frequencies [64]. The medium strong band in FT-IR spectrum at 1252–1228 cm^{-1} is assigned to O–H in-plane bending vibration for both the O–H groups in the ring. The theoretically computed value at 1290–1201 cm^{-1} by B3LYP/6-31G(d) method show very good agreement with recorded spectrum.

The O–H out-of-plane bending mode for the free molecule lies below 300 cm^{-1} and it is beyond the infrared spectral range of the present investigation. However, for the associated molecule[62], the O–H out-of-plane bending mode lies in the region 517–710 cm^{-1} in both intermolecular and intramolecular associations, the frequency is at a higher value than in free O–H. The theoretically computed value by B3LYP/6-31G(d) method at 695–693 cm^{-1} are assigned to O–H out-of-plane bending vibration. Yet again, this situation may be evidence that the hydrogen bonds.

3.4.4. N–H vibrations

The characteristic secondary amide bands in the stretching region, associated with N–H stretch and the overtone of N–H in-plane bending, can be observed in the IR spectrum. The major vibrational spectral effect of the intermolecular amide hydrogen bonding can be found in the N–H stretching mode. The strong band of N–H stretching extends from 3400 to 3100 cm^{-1}, with the centre of the band at 3370 cm^{-1} [59,66,67]. The calculated wavenumber of the above mode is at 3502 cm^{-1} for the B3LYP/6-31G(d) method. The strong band in the FT-IR spectrum at 3185 cm^{-1} also supports the formation of a strong N–H···N hydrogen bond. The lowering of the N–H stretching wavenumber can be attributed to the red shifting due to intermolecular N–H···N interaction. The red shifting is further enhanced by the reduction in the N–H bond order values, occurring due to donor–acceptor interaction. The first overtone of the N–H in-plane bending mode (~3110 cm^{-1}) falling on the N–H stretching band positions produces two bands of comparable intensities, equally displaced on either side of this wavenumber

resulting from Fermi resonance with one or more N–H stretching [59].

3.4.5. C=N, C–N and N–N vibrations

Three bonds, viz. C–H, C=N and N–N and each has a well known characteristic vibrational frequency of its own. N–N stretching vibration, which due to its symmetry has a very characteristic and they are difficult to observe in the infrared spectrum. But the change of N–N bond length in the molecule which has two unequivalent C=N parts causes a change in dipole moment. Thus the N–N stretching mode is IR active and is predicted to be medium strength. The band occurring between 1450 and 1380 cm^{-1} corresponds to the N=N stretching of an azo (N–N) compound [68]. C–N stretching vibrations of azo compounds are expected to occur in the region 1200–1130 cm^{-1} [69,70]. These bands shift in wavenumber and intensity in a complex fashion, depending on the neighbouring groups, conjugation effects, H-bonding and molecular tautomerism [70]. In our case, the substituents of title compound influence both the wavenumber and intensity. The medium band in FT-IR at 1548 $cm^{-1}$are attributed to the N–N stretching vibration of the molecule. The azo stretching vibration undergoes a large downshift in wavenumber due to greater conjugation and π-electron delocalization [71]. The theoretical calculation by B3LYP method predicts the above said vibration at 1540 cm^{-1} exactly correlates with experimental findings.

3.4.6. CH_3 and C–O vibrations

The title molecule under consideration possesses one CH3 unit which lies in the terminal group of molecule. For the assignments of CH3 group frequencies one can expect nine fundamentals can be associated to each CH3 group. Methyl group vibrations are generally referred to as electron-donating substituent in the aromatic rings system, the antisymmetric C–H stretching mode of CH3 is expected around 2980 cm^{-1} and CH3 symmetric stretching is expected at 2870 cm^{-1} [72,73]. The first of these results from the antisymmetric stretching of CH3 mode in which the two C–H bonds of the methyl group are expanding while the third one is contracting. The second arises from the symmetric stretching, in which all the three C–H bonds expand and contract in phase. The antisymmetric and symmetric stretching vibrations are observed in the 2993 and 2869 cm^{-1} regions respectively. In our present work, the antisymmetric stretching vibrations of CH3 group predicted by B3LYP/6-31G(d) method at 3028 cm^{-1}. The symmetric stretching vibration of CH3 group is predicated theoretically at 2959–2822 cm^{-1} by B3LYP/6-31G(d) method. The weak intense bands in IR spectrum at 667 cm^{-1} are attributed to the CH3 rocking mode. The methyl twisting mode of vibration coupled with methylene group. The other CH3 wagging mode and CH3 scissoring vibrations are also predicted theoretically at 1160 and 1023 cm^{-1} for B3LYP/6-31G(d) method. The C–O stretching band of the aromatic ether in IR spectrum is characterized by the frequencies around 1270–1230 cm^{-1}. According to our calculations, the theoretical frequencies around 1240 cm^{-1} for HF/6-31G(d) and 1211 cm^{-1} on B3LYP/6-31G(d) methods with strong IR intensities correspond satisfactorily to experimental data (1277 cm^{-1} in FT-IR spectrum).

3.4.7. Low wavenumber vibrations of hydrogen bonds

The attractive interaction between the hydrogen donor group and the accept or moiety leads to the occurrence of new vibrational degrees of freedom, the so-called hydrogen bond modes [74]. Such modes are connected with elongations changing the X···Y(O···O, N···N and O···N) distance and/or the relative orientation of the hydrogen bonded groups. Thus, they provide direct insight into the structure of hydrogen bonds and into processes of bond formation and cleavage. As such modes are characterized by a high reduced mass of the oscillator and a small force constant determined by the comparably weak attractive interaction along the hydrogen bond, hydrogen bond modes occur at low wavenum-

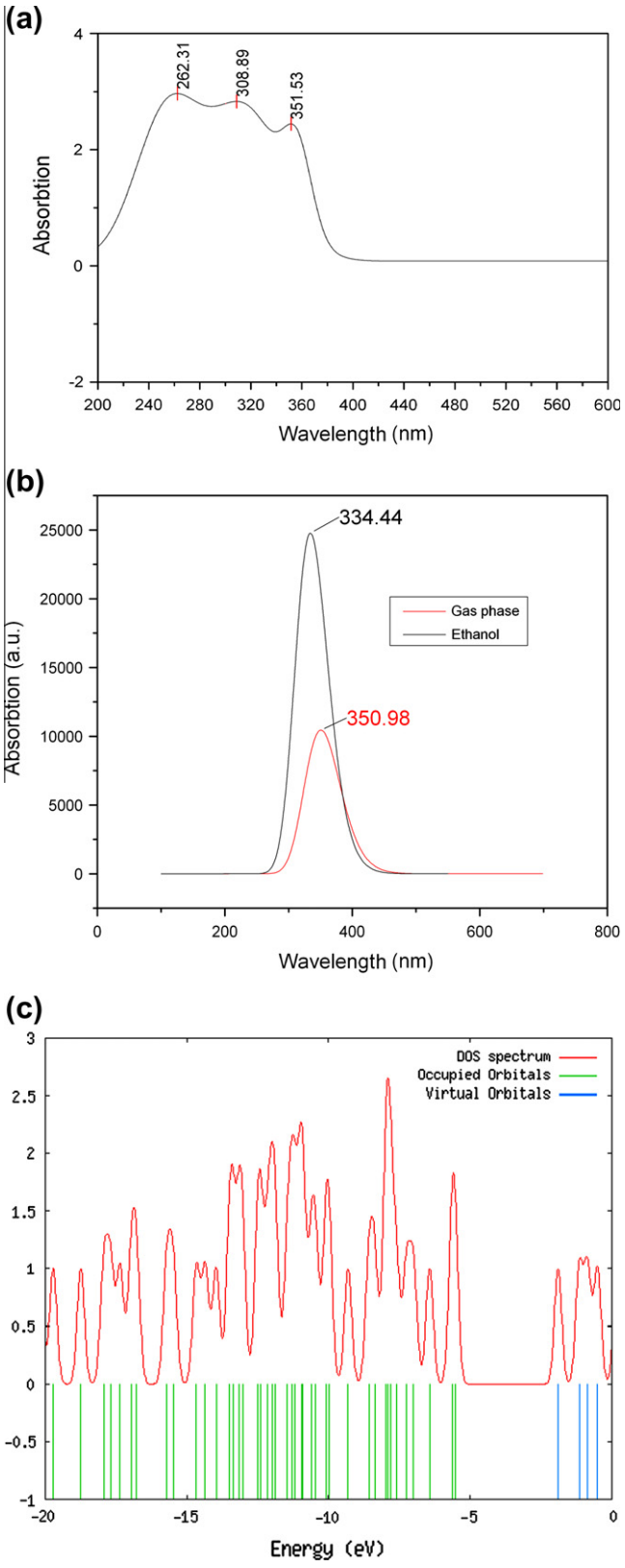

Fig. 10. (a) Experimental Uv–vis spectrum. (b) Theoretical Uv–vis spectrum using TD-DFT 6-31G(d). (c) The frontier molecular orbital energies and corresponding DOS spectrum of the title compound.

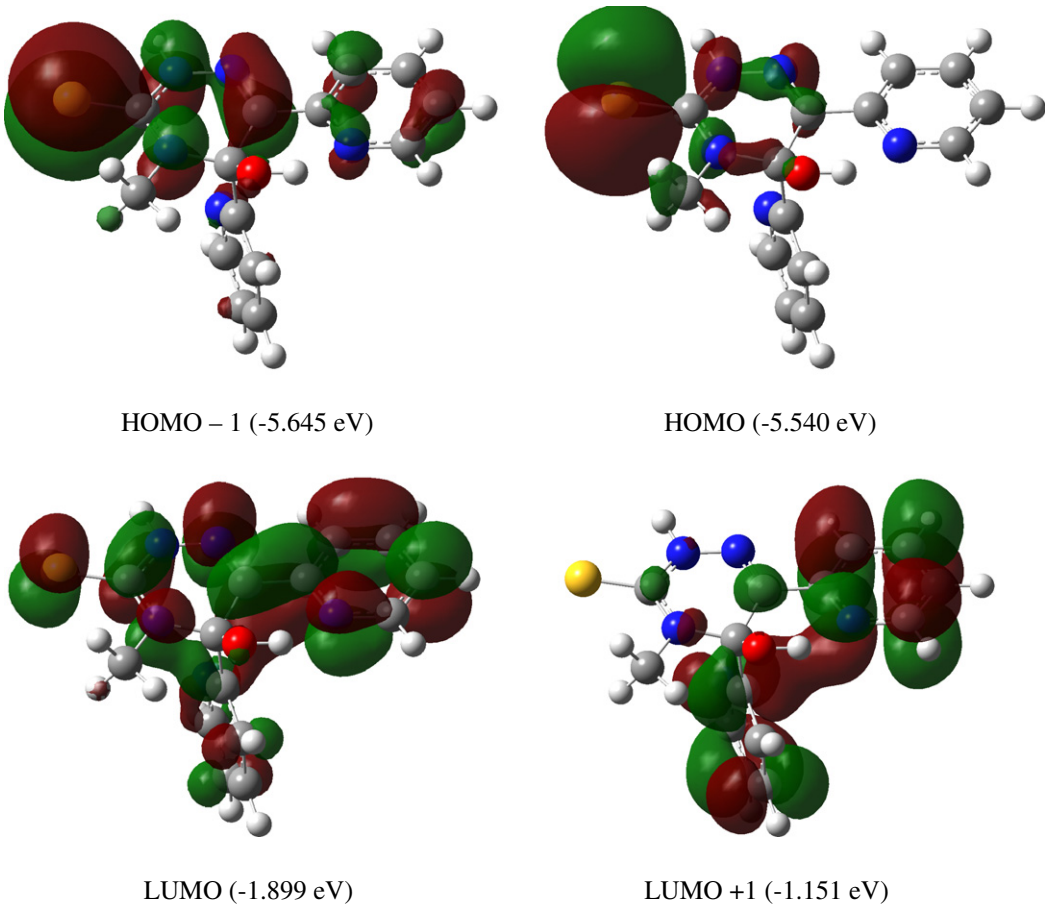

Fig. 11. Molecular orbital surfaces and energy levels given in parentheses for the HOMO − 1, HOMO, LUMO and LUMO + 1 of the title compound computed at B3LYP/6-31G(d) level.

Table 7
Atomic charges (*e*) of the title compound in gas phase and solution phase.

Atom	In gas phase		In solution phase B3LYP/6-31G(d)		
	HF/6-31G(d)	B3LYP/6-31G(d)	Chloroform(ε = 4.9)	Ethanol(ε = 24.55)	Water(ε = 78.39)
C1	0.06137	0.03342	0.03834	0.03803	0.03796
C2	−0.22195	−0.13686	−0.14543	−0.14552	−0.14553
C3	−0.25447	−0.13863	−0.1386	−0.13826	−0.13818
C4	−0.1471	−0.10338	−0.10053	−0.10014	−0.10006
C5	0.54783	0.40688	0.41212	0.41829	0.41957
C6	0.14662	0.1513	0.25916	0.26084	0.2612
C7	0.30281	0.27576	0.32783	0.32779	0.32778
C8	−0.25508	−0.14036	−0.14676	−0.14516	−0.14481
C9	0.24901	0.27693	0.314	0.31391	0.31389
C10	−0.14694	−0.10251	−0.1019	−0.101886	−0.10188
C11	0.53733	0.34717	0.342	0.34154	0.34144
C12	−0.22705	−0.15473	−0.17465	−0.17501	−0.17508
C13	0.06716	0.04122	0.05384	0.05375	0.05375
C14	−0.30732	−0.32527	−0.3141	−0.31248	−0.31213
S1	−0.3002	−0.27605	−0.3567	−0.3815	−0.38671
O1	−0.76573	−0.63617	−0.66921	−0.6702	−0.6704
N1	−0.55786	−0.4683	−0.47666	−0.47896	−0.47945
N2	−0.58661	−0.44339	−0.4379	−0.43857	−0.43869
N3	−0.22885	−0.25502	−0.31845	−0.32019	−0.32057
N4	−0.66987	−0.42336	−0.42851	−0.42829	−0.42823
N5	−0.56503	−0.47084	−0.56881	−0.56996	−0.57021

bers in the range between 50 and 300 cm^{-1}. In addition, a substantial spread of vibrational wavenumber occurs for liquids with a multiple hydrogen bonding geometries, resulting in a pronounced inhomogeneous broadening of the vibrational bands. The lattice vibrations of rotatory type are generally stronger in intensity than the translatory type.

Theoretical and experimental results of the title compound are shown in Table 5. The vibrational bands assignments have been made by using Gauss-View Molecular Visualization program (Fig. 8b). To make comparison with experiment, we present correlation graphics in Fig. 9 based on the calculations. As we can see from correlation graphic in Fig. 9 experimental fundamentals are

Table 8
Total energies and dipole moments of the title compound in different solvent.

Method	ε	Energy (a.u.)	ΔE (kcal/mol)	μ (D)
B3LYP Onsager	1	−1288.4634018		7.6721
	4.9	−1288.4686036	−3.2643	10.1550
	10.36	−1288.4700208	−4.1535	10.8235
	24.55	−1288.4708995	−4.7061	11.2362
	46.37	−1288.4712318	−4.9134	11.3920
	78.39	−1288.4713858	−5.0100	11.4640
PCM	4.9	−1288.4807971	−10.9155	10.1442
	10.36	−1288.4848534	−13.4607	10.7069
	24.55	−1288.4872896	−14.9899	11.0384
	46.37	−1288.4882400	−15.5861	11.1630
	78.39	−1288.4894755	−16.3617	11.2475

$\Delta E = E_{solvation} - E_{gas}$, ε = dielectric constant.

in better agreement with the scaled fundamentals and are found to have a better correlation for B3LYP than HF.

3.5. NMR spectra

The ^{1}H NMR and ^{13}C NMR spectra was recorded on a Varian Mercury spectrometer using tetramethylsilane (TMS) as internal reference. GIAO ^{1}H and ^{13}C chemical shift calculations have been carried out using the HF and B3LYP methods with 6-31G(d) basis set for the optimized geometry. The results of these calculations are tabulated in Table 6. Since experimental ^{1}H chemical shift values were not available for individual hydrogen, we have presented the average values for aromatic CH and CH_3 hydrogen atoms.

Due to deshielded by the electronegative property of N3, N4 and S1 atoms, the chemical shift value of C7 which has bigger value than the others, have observed 171.22 at. Similarly, six carbons peaks in the ring are calculated from 122.38 to 160.28 ppm. Besides, due to shielding effect which the non-electronegative property of hydrogen atom, the chemical shift value of C14 atom is lower than the others carbon peak. ^{1}H atom is the smallest of all atoms and is mostly localized on periphery of the molecules; therefore their chemical shifts would be more susceptible to intermolecular interactions in the aqueous solutions as compared to that for other heavier atoms.

The formation of hydrogen bonds leads to a significant downfield shift of the isotropic chemical shifts. If hydrogen-bond formation involves amide protons and the carbonyl group, the direction of the electron density shift from the NH to the carbonyl group results in a decreased magnetic shielding for the amide proton and hence results in a shift to lower field of its proton signal [75,76]. Therefore, the experimental chemical shift value of H(NH) (8.04 ppm) is smaller than H(OH) (12.0 ppm). In this study, there is good agreement between experimental and theoretical chemical shift results.

Another important aspect is that, hydrogen attached or nearby electron withdrawing atom or group can decrease the shielding and moves the resonance of attached proton towards to a higher frequency. By contrast electron donating atom or group increases the shielding and moves the resonance towards to a lower frequency. The chemical shifts obtained and calculated for the hydrogen atoms of methyl groups are quite low. All values are $\leqslant$3 ppm [77] due to shielding effect. It is true from above literature data in our present study the methyl protons at C14 appears as singlet with three proton integral at 2.91 ppm shows good agreement with computed chemical shift values are shown in Table 6.

Comparing calculational and the experimental data, we studied the relativity between the calculation and the experiments and obtained that the linear function formula is $y = 1.106 \times -12.471$ for HF; where R^2 is 0.9785, and $y = 0.9499x + 1.048$ for B3LYP; where R^2 is 0.9858. According to these results, it is seen that, the results of HF method have shown better fit to experimental ones than B3LYP in evaluating ^{1}H and ^{13}C chemical shifts.

3.6. Electronic absorption spectra

Electronic absorption spectra were measured on a Unicam UV–VIS spectrophotometer in ethanol. The UV–visible spectrum of O-hydroxylated Schiff bases that exist mainly as phenol–imine structure indicates the presence of a band at <400 nm, whereas compounds exist as keto–mine form show a new band, especially in polar and nonpolar solvents at >400 nm [78–86]. Experimentally, electronic absorption spectra of the title compound in ethanol solvent showed three bands at 262.31, 308.89 and 351.53 nm (Fig. 10a), which correspond to phenol–imine form. According to experimental results, the phenol–imine form is dominant in chloroform solvent, which has absorption band at 262.31 nm with log ε = 3.49. This value is similar to those found in related compounds [87–89].

Electronic absorption spectra were calculated by using TD-DFT method based on the B3LYP/6-31G(d) level optimized structure in gas phase. The predicted absorption wavelength is at 350.98 nm with the oscillator strength being 0.2561 for TD-DFT calculation (Fig. 10b). It is obvious that to use TD-DFT calculations to predict the electronic absorption spectra is a quite reasonable method. In addition to the calculations in gas phase, TD-DFT calculations of the title compound in ethanol solvent were performed by using PCM model. The PCM calculation reveals that the calculated absorption band has red shift with a value 334.44 nm with oscillator strength being 0.599. The reason for this red shift is solvent effect which can affect the geometry and electronic structure as well as the properties of the molecule as solvent effects induce the lower energy of the molecules, and generate more significant red shift for absorption bands [90]. For the title compound, TD-DFT method for both in gas phase and solvent media is convenient to predict the electronic absorption spectra.

According to the TD-DFT calculational electronic absorption spectra, the maximum absorption wavelength corresponding to the electronic transition is from the highest occupied molecular orbital (HOMO) to the lowest unoccupied molecular orbital (LUMO). The frontier molecular orbitals energies and corresponding density of state of the title compound shown in Fig. 10c.

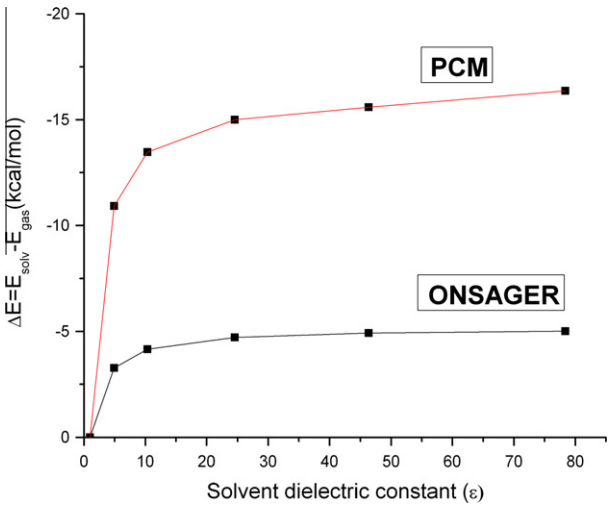

Fig. 12. Energy difference between the gas phase and solvent media by PCM and Onsager methods at B3LYP/6-31G(d) level of theory.

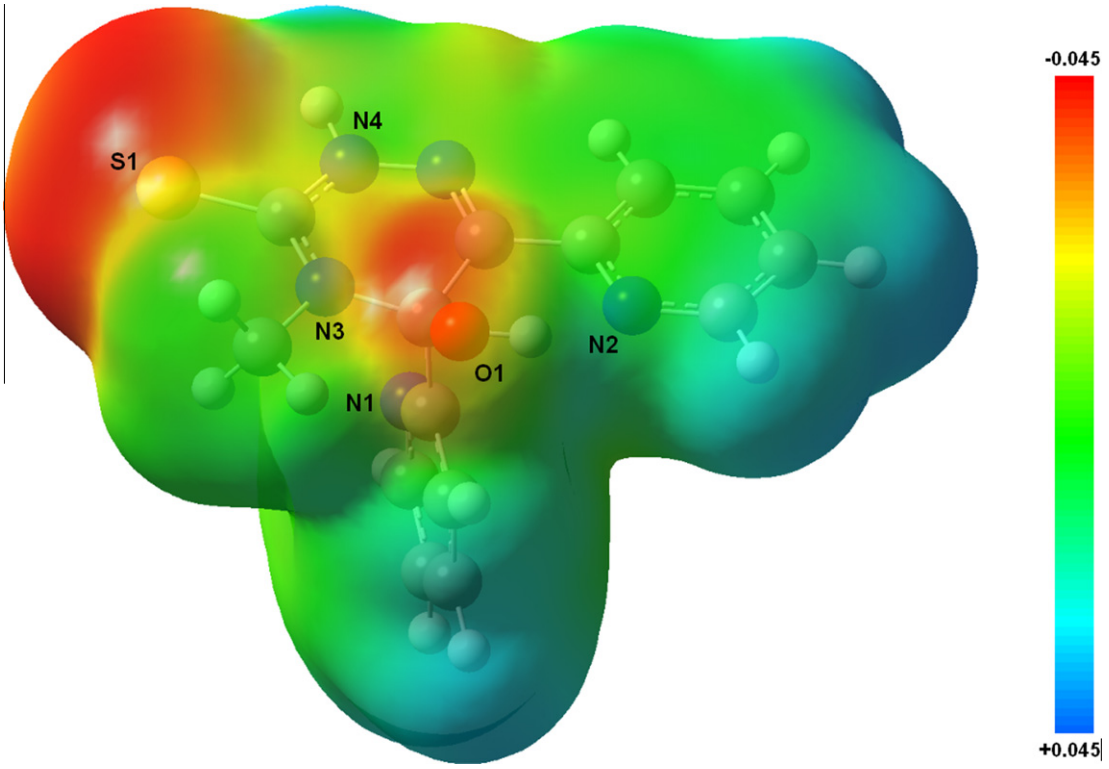

Fig. 13. Molecular electrostatic potential map calculated at B3LYP/631G(d) level.

The frontier molecular orbitals of the title compound are partly or mainly localized on the cresol fragment and pyrazoline ring. Molecular orbital coefficients analyses based on optimized geometry indicate that, for the title compound, the frontier molecular orbitals are mainly composed of *p*-atomic orbitals, so aforementioned electronic transitions are mainly derived from the contribution of bands π–π*.

3.7. Frontier molecular orbitals

The frontier molecular orbitals play an important role in the electric and optical properties, as well as in UV–Vis spectra and chemical reactions [91,92]. Fig. 11 shows the distributions and energy levels of the HOMO − 1, HOMO, LUMO and LUMO + 1 orbitals computed at the B3LYP/6-31G(d) level for the title compound. The calculations indicate that the title compound has 78 occupied molecular orbitals. Both the highest occupied molecular orbitals (HOMOs) and the lowest-lying unoccupied molecular orbitals (LUMOs) are mainly localized on the rings indicating that the HOMO–LUMO are mostly the π-antibonding type orbitals. As seen from Fig. 11, the HOMO-1 and HOMO orbitals are mainly delocalized on the S atom and triazine group, while the LUMO and LUMO + 1 orbitals are mainly delocalized on triazine group and pyridine rings. Namely, electron transitions are corresponding to the $n \rightarrow \pi^*$ and $\pi \rightarrow \pi^*$ electron transitions. The value of the energy separation between the HOMO and LUMO is 3.64 eV and this large energy gap indicates that the title structure is quite stable.

3.8. Atomic charge distributions in gas-phase and in solution-phase

The Mulliken atomic charges for the non-H atoms of the title compound were calculated at HF/6-31G(d) and B3LYP/6-31G(d) level in gas phase. In addition, to investigate the solvent effect for the atomic charge distributions of the title compound, based on the B3LYP/6-31G(d) model and the Onsager model, three kinds of solvent ($\varepsilon = 78.39$, H_20; $\varepsilon = 24.55$, C_2H_5OH; $\varepsilon = 4.9$, $CHCl_3$) were selected and calculated values were also listed in Table 7. The

Table 9
The electric dipole moment μ (D), the average polarizability α_0 ($\times 10^{-24}$ esu) and first hyperpolarizability β_0 ($\times 10^{-33}$ esu) of title compound.

μ_x	−2.74	β_{xxx}	−21788.31
μ_y	1.26	β_{yyy}	941.08
μ_z	−0.17	β_{zzz}	−134.86
μ	7.98	β_{xyy}	−1144.97
α_{xx}	42.47	β_{xxy}	3961.21
α_{yy}	27.02	β_{xxz}	1822.03
α_{zz}	23.15	β_{xzz}	101.86
α_{xy}	−3.87	β_{yzz}	83.80
α_{xz}	−1.77	β_{yyz}	−455.03
α_{yz}	3.59	β_{xyz}	−211.66
α_0	30.88	β_0	23072.06

Table 10
Calculated energies (a.u), zero-point vibrational energies (kcal mol^{-1}), rotational constants (GHz), entropies (cal mol^{-1} K^{-1}) and dipole moment (D) of the title compound.

Parameters	6-31G(d)	
	HF	B3LYP
Dipole moment (D)	9.5104	7.6721
Zero-point vibrational energy(kcal mol^{-1})	162.11504	150.35863
Total energy (a.u.)	−1282.31769	−1288.46340
Rotational constants	0.41098	0.40138
	0.25386	0.24981
	0.19331	0.19130
Entropy (cal mol^{-1} K^{-1})		
Rotational	30.554	30.600
Translational	38.591	38.591
Vibrational	49.625	53.161
Total	118.769	122.350

Mulliken atomic charges shows that the N1, N2 and N4 atoms and triazine ring oxygen atom O1 have bigger negative atomic charges [−0.4683e (Mulliken) for N1, −0.44339e (Mulliken) for N2, −0.42336e (Mulliken) for N4 and −0.63617e (Mulliken) for O1], calculated at B3LYP/6-31G(d) level in gas phase. This behaviour can be the result of intramolecular O1–H1···N2 hydrogen bonds. On the other hand, it can be found that in solution-phase, the atomic charge values of the O1, N1, N3, N4 and N5 atoms are bigger than those in gas-phase and while their atomic charge values will increase with the increase of the polarity of the solvent, that value of N2 decrease with the increase of the solvent polarity. This result reveals that the coordinate ability of O1, N1/N5 atoms will be changed in different solvents, which may be helpful when one wants to use the title compound to construct interesting metal complexes with different coordinate geometries [93]. This calculated result is not only consistent with many reported experimental facts [94–96], it also supports the original idea of our synthesis.

3.9. Total energies and dipol moments

To evaluate the energetic behaviour of the title compound in solvent media, we carried out calculations in five kinds of solvent (ε = 78.39, H_20; ε = 46.7, DMSO; ε = 24.55, C_2H_5OH; ε = 10.36, CH_2C1CH_2C1; ε = 4.9, $CHC1_3$). Total energies and dipole moments were calculated in solvent media at B3LYP/6-31G (d) level using Onsager and PCM models and the results are presented in Table 8. According to Table 8, we can conclude that the total energies of the title compound obtained by Onsager and PCM methods decrease with the increasing polarity of the solvent, while the stability of the title compound increases in going from the gas phase to the solution phase. The energy difference between the gas phase and solvent media is given in Fig. 12 for both methods. As can be seen from Fig. 12, the PCM method provided a more stable structure than Onsager's method (10 kcal/mol on average).

3.10. Molecular electrostatic potential

MEP is related to the electronic density and is a very useful descriptor in understanding sites for electrophilic attack and nucleophilic reactions as well as hydrogen bonding interactions [97,98]. The electrostatic potential $V(r)$ is also well suited for analyzing processes based on the "recognition" of one molecule by another, as in drug-receptor, and enzyme–substrate interactions, because it is through their potentials that the two species first "see" each other [99,100].

To predict reactive sites of electrophilic and nucleophilic attack for the investigated molecule, MEP at the B3LYP/6-31G(d) optimized geometry was calculated. The negative (red and yellow) regions of MEP were related to electrophilic reactivity and the positive (blue) regions to nucleophilic reactivity (see Fig. 13). As can be seen in Fig. 13, there are two possible sites of electrophilic attack. The negative regions are mainly localized on the carbonyl oxygen atoms, O1, and S1 atom. Also, a negative electrostatic potential region is observed around the N1 atom. The negative $V(r)$ values are −0.045 a.u. for S1 atom, which is the most negative region: About −0.037 for O1 atom and −0.042 a.u. for N1 atom, which is the less negative region. However, a maximum positive region is localised on atom N4, probably due to the hydrogen, with a maximum value of +0.045 a.u. These results provide information concerning the region where the compound can interact intermolecularly and bond metallically. Therefore, Fig. 13 confirms the existence of an intermolecular N–H···N interaction between the protonated and unprotonated N, O and S atoms. According to these calculated results, the MEP map shows that the negative potential sites are on electronegative atoms as well as the positive potential sites are around the hydrogen atoms. These sites give information about the region from where the compound can have noncovalent interactions.

3.11. Non-linear optical effects

Polarizabilities and hyperpolarizabilities characterize the response of a system in an applied electric field [101]. They determine not only the strength of molecular interactions (long-range intermolecular induction, dispersion forces, etc.) as well as the cross sections of different scattering and collision processes, but also the non-linear optical properties (NLO) of the system [102,103]. It has been found that the dye sensitizer hemicyanine system, which has high NLO property, usually possesses high photoelectric conversion performance [104]. In order to investigate the relationships among photocurrent generation, molecular structures and NLO, the polarizabilities and hyperpolariz-abilities of title compound was calculated.

The first hyperpolarizability (β_0) of this novel molecular system, and related properties (β, α_0 and $\Delta\alpha$) of title compound are calculated using B3LYP/6-31G(d) basis set, based on the finite-field approach. In the presence of an applied electric field, the energy of a system is a function of the electric field. First hyperpolarizability is a third rank tensor that can be described by a 3 × 3 × 3 matrix. The 27 components of the 3D matrix can be reduced to 10 components due to the Kleinman symmetry [105]. It can be given in the lower tetrahedral format. It is obvious that the lower part of the 3 × 3 × 3 matrix is a tetrahedral. The components of β are defined as the coefficients in the Taylor series expansion of the energy in the external electric field. When the external electric field is weak and homogeneous, this expansion becomes:

$$E = E^0 - \nu_\alpha F_\alpha - 1/2\alpha_{\alpha\beta}F_\alpha F_\beta - 1/6\beta_{\alpha\beta\gamma}F_\alpha F_\beta F_\gamma + \cdots$$

where E^0 is the energy of the unperturbed molecules, F_α the field at the origin μ_α, $\alpha_{\alpha\beta}$ and $\beta_{\alpha\beta\gamma}$ are the components of dipole moment, polarizability and the first hyperpolarizabilities, respectively. The total static dipole moment μ, the anisotropy of the polarizability $\Delta\alpha$ and the mean first hyperpolarizability β_0, using the x, y, z components they are defined as:

$$\mu = (\mu_x^2 + \mu_y^2 + \mu_z^2)^{1/2}$$

$$\alpha_0 \frac{\alpha_{xx} + \alpha_{yy} + \alpha_{zz}}{3}$$

$$\Delta\alpha = \left[\frac{(\alpha_{xx} - \alpha_{yy})^2 - (\alpha_{yy} - \alpha_{zz})^2 - (\alpha_{zz} - \alpha_{xx})^2}{2}\right]^{1/2}$$

$$\beta_0 = \left[(\beta_{xxx} + \beta_{xyy} + \beta_{xzz})^2 + (\beta_{yyy} + \beta_{yxx} + \beta_{yzz})^2 + (\beta_{zzz} + \beta_{zxx} + \beta_{zyy})^2\right]^{1/2}$$

Since the values of the polarizabilities α and hyperpolarizability β of Gaussian03 output are reported in atomic units (a.u.), the calculated values have been converted into electrostatic units (esu) (α: 1 a.u. = 0.1482×10^{-24} esu; β: 1 a.u. = 8.6393×10^{-33} esu). In Table 5 are listed the B3LYP/6-31G(d) results of the electronic dipole moment μ_i = (i = x, y, z) polarizability α_0 and the first hyperpolarizability β_0 for title compound The calculated dipole moment is equal to 7.98 D. For direction x, y and z, these values are equal to −2.74 D, 1.26 D and −0.17 D, respectively. The calculated polarizability α_0, is equal to 30.88×10^{-24} esu. As we can see in Table 9. The first hyperpolarizability value β_0 of the title compound is equal to 23072.06×10^{-33} esu. The hyperpolarizability β dominated by the longitudinal components of β_{xxx}, β_{yyy}, β_{xxy}, β_{yyz}, and β_{xyy}. Large

values of particular components of polarizability and hyperpolarizability indicate substantial delocalization of charges in these directions.

Many research works have indicated that the frontier molecular orbitals (FMOs) have significant effect on material NLO properties [106–109]. To understand this phenomenon in the context of molecular orbital picture, we examined the molecular HOMOs and molecular LUMOs of the title compound and showed in Fig. 11.

3.12. Thermodynamic parameters of the title compound

Several thermodynamic parameters have been calculated using HF, BLYP and B3LYP with 6-31G(d) basis set and calculated these parameters of the title compound are given in Table 10. Accurate prediction of zero-point vibrational energy (ZPVE) and the entropy (Svib(T)) scaling the data [110]. The total energies and the change in the total entropy of the title compound at room temperature at different theoretical methods are also presented. In Table 6 demonstrates several thermodynamic parameters of the title compound without of results of experimental.

4. Conclusions

In this study, we have synthesised a novel benzimidazole compound, $C_{14}H_{13}N_5OS$, and characterised it using spectroscopic (FT-IR and NMR) and structural (XRD) techniques. The X-ray structure is found to be very slightly different from its optimized counterparts, and the crystal structure is stabilised by a N–H···N-type hydrogen bond between the protonated and unprotonated N atoms of adjacent triazine rings as well as by van der Waals forces. The results of the HF method show a better fit to experimental values than B3LYP in evaluating geometrical parameters. It is noted here that the experimental results are for the solid phase and the theoretical calculations are for the gaseous phase. In the solid state, the existence of the crystal field together with the intermolecular interactions holds the molecules together, which results in differences between the calculated and experimental values for the bond parameters. Despite the differences observed in the geometric parameters, the general agreement is good and the theoretical calculations support the solid-state structures. However, it can be seen from the theoretical results that the B3LYP method is more appropriate than the HF method for the calculation of vibrational frequencies and chemical shifts. The MEP map shows that the negative potential sites are on electronegative atoms as well as the positive potential sites are around the hydrogen atoms. These sites give information about the region from where the compound can have intramolecular interactions. The total energy of the title compound decreases with increasing polarity of the solvent and the stability of the title compound increases in going from the gas phase to the solution phase. The value of the energy separation between the HOMO and LUMO is very large and this energy gap gives significant informations about the title compound. The non-linear optical properties are also addressed theoretically. The predicted NLO properties of the title compound are much greater than ones of urea. The title compound is a good candidate as second-order NLO material. I hope this paper will be helpful for the design and synthesis new materials.

Supplementary material

CCDC – 763860 contains the supplementary crystallographic data for the compound reported in this paper. These data can be obtained free of charge at www.ccdc.cam.ac.uk/conts/retrieving.html [or from the Cambridge Crystallographic Data Centre (CCDC), 12 Union Road, Cambridge CB2 1EZ, UK; fax: +44 (0)1223 336033; e-mail: deposit@ccdc.cam.ac.uk].

Acknowledgement

This study was supported financially by the Research Centre of Ondokuz Mayıs University (Project No: F-461).

References

[1] J. Janczak, R. Kubiak, Acta Chem. Scand. 53 (1999) 606–610.
[2] J. Janczak, G.J. Perpétuo, Acta Cryst. C 57 (2001) 123–125.
[3] J. Janczak, G.J. Perpétuo, Acta Cryst. C 57 (2001) 873–875.
[4] J. Janczak, G.J. Perpétuo, Acta Cryst. C 57 (2001) 1120–1122.
[5] J. Janczak, G.J. Perpétuo, Acta Cryst. C 57 (2001) 1431–1433.
[6] J. Janczak, G.J. Perpétuo, Acta Cryst. C 58 (2002) 112–114.
[7] J.P. Mathias, E.E. Siemanek, J.A. Zerkowski, Ch.T. Seto, G.M. Whitesides, J. Am. Chem. Soc. 116 (1994) 4316–4325.
[8] J.A. Zerkowski, G.M. Whitesides, J. Am. Chem. Soc. 116 (1994) 4298–4304.
[9] J.C. MacDonald, G.M. Whitesides, Chem. Rev. 94 (1994) 2383–2420.
[10] T.N.G. Row, Coord. Chem. Rev. 183 (1999) 81–100.
[11] M.J. Krische, J.M. Lehn, Struct Bond. 96 (2000) 3–29.
[12] D. C Sherrington, K.A. Taskinen, Chem. Soc. Rev. 30 (2001) 83–91.
[13] S.B. Holla, B.K. Sarojini, K. Shridhara, G. Antony, Il Farmaco 54 (1999) 149–151.
[14] G.S. Gruzdyev, V.A. Zinchenko, V.A. Kalinin, R.I. Slovtsov, The Chemical Protection of Plants, Mir Publishers, Moscow, 1983.
[15] M. Mashaly, H.A. Bayoumi, A. Taha, J. Serb. Chem. Soc. 64 (1999) 621–635.
[16] M.G.B. Drew, D. Guillaneux, M.J. Hudson, P.B. Iveson, C. Madic, Inorg. Chem. Commun. 4 (2001) 462–466.
[17] M.G.B. Drew, D. Guillaneux, M.J. Hudson, P.B. Iveson, M.L. Russell, C. Madic, Inorg. Chem. Commun. 4 (2001) 12–15.
[18] M.G.B. Drew, M.J. Hudson, P.B. Iveson, C. Madic, Acta Cryst. C 56 (2000) 434–435.
[19] M.G.B. Drew, M.J. Hudson, P.B. Iveson, C. Madic, M.L. Russell, J. Chem. Soc. Dalton Trans. (2000) 2711–2720.
[20] J. Casanovas, A.M. Namba, S. Leon, G.L.B. Aquino, G.V.J. da Silva, C. Aleman, J. Org. Chem. 66 (11) (2001) 3775–3782.
[21] J. Org. Chem. 66 (24) (2001) 7967–7973.
[22] D.A. Forsyth, A.B. Sebag, J. Am. Chem. Soc. 119 (1997) 9483–9494.
[23] T. Helgaker, M. Jaszunski, K. Ruud, Chem. Rev. 99 (1999) 293–352.
[24] R. Ditchfleld, J. Chem. Phys. 56 (1972) 5688–5691.
[25] K. Wolinski, J.F. Hinton, P. Pulay, J. Am. Chem. Soc. 112 (1990) 8251–8260.
[26] J.R. Cheeseman, G.W. Trucks, T.A. Keith, M.J. Frisch, J. Chem. Phys. 104 (1996) 5497–5509.
[27] P. Cimino, L. Gomez-Paloma, D. Duca, R. Riccio, G. Bifulco, Magn. Reson. Chem. 4 (2004) 26–33.
[28] R.A. Friesner, R.B. Murphy, M.D. Beachy, M.N. Ringnalda, W.T. Pollard, B.D. Dunietz, Y. Cao, J. Phys. Chem. A 103 (1999) 1913–1928.
[29] L. Rufisek, Z. Havlas, Int. J. Quantum Chem. 91 (2003) 504–510.
[30] T. Ziegler, Chem. Mater. Sci. 55 (1997) 69.
[31] Stoe & Cie X-AREA (Version 1.18) X-RED32 (Version 1.04) Stoe&Cie, Darmstadt, Germany, 2002.
[32] G.M. Sheldrick, SHELXS97, SHELXL97, University of Gottingen, Germany, 1997.
[33] C. Lee, W. Yang, R.G. Parr, Phys. Rev. B 37 (1988) 785–789.
[34] A.D. Becke, J. Chem. Phys. 98 (1993) 5648–5652.
[35] R. Ditchfield, W.J. Hehre, J.A. Pople, J. Chem. Phys. 54 (1971) 724–728.
[36] J.B. Foresman, A. Frisch, Exploring Chemistry with Electronic Structure Methods, second ed., Gaussian Inc., Pittsburgh, 1996.
[37] R. Ditchfield, J. Chem. Phys. 56 (1972) 5688–5691.
[38] RII. Dennington, T. Keith, J. Millam, GaussView, Version 4.1.2. Semichem Inc., Shawnee Mission, KS, 2007.
[39] A. Frisch, RII. Dennington, T. Keith, J. Millam, A.B. Nielsen, A.J. Holder, J. Hiscocks, GaussView Reference, Version 4.0. Gaussian Inc., Pittsburgh, 2007.
[40] M.J. Frisch, G.W. Trucks, H.B. Schlegel, G.E. Scuseria, M.A. Robb, J.R. Cheeseman, J.A. Montgomery, Jr., T. Vreven, K.N. Kudin, J.C. Burant, J.M. Millam, S.S. Iyengar, J. Tomasi, V. Barone, B. Mennucci, M. Cossi, G. Scalmani, N. Rega, G.A .Petersson, H. Nakatsuji, M. Hada, M. Ehara, K. Toyota, R. Fukuda, J. Hasegawa, M. Ishida, T. Nakajima, Y. Honda, O. Kitao, H. Nakai, M. Klene, X. Li, J.E. Knox, H.P. Hratchian, J.B. Cross, V. Bakken, C. Adamo, J. Jaramillo, R. Gomperts, R.E. Stratmann, O. Yazyev, A.J. Austin, R. Cammi, C. Pomelli, J.W. Ochterski, P.Y. Ayala, K. Morokuma, G.A. Voth, P. Salvador, J.J. Dannenberg, V.G. Zakrzewski, S. Dapprich, A.D. Daniels, M.C. Strain, O. Farkas, D.K. Malick, A.D. Rabuck, K. Raghavachari, J.B. Foresman, J.V. Ortiz, Q. Cui, A.G. Baboul, S. Clifford, J. Cioslowski, B.B. Stefanov, G. Liu, A. Liashenko, P. Piskorz, I. Komaromi, R.L. Martin, D.J. Fox, T. Keith, M.A. Al-Laham, C.Y. Peng, A. Nanayakkara, M. Challacombe, P.M.W. Gill, B. Johnson, W. Chen, M.W. Wong, C. Gonzalez, J.A. Pople, Gaussian Inc., Wallingford CT, 2004.
[41] E. Cances, B. Mennucci, J. Tomasi, J. Chem. Phys. 107 (1997) 3032.
[42] L. Onsager, J. Am. Chem. Soc. 58 (1936) 1486.
[43] S. Miertus, E. Scrocco, J. Tomasi, Chem. Phys. 55 (1981) 117.
[44] V. Barone, M. Cossi, J. Phys. Chem. A 102 (1998) 1995.

[45] M. Cossi, N. Rega, G. Scalmani, V. Barone, J. Comput. Chem. 24 (2003) 669.
[46] J. Tomasi, B. Mennucci, R. Cammi, Chem. Rev. 105 (2005) 2999.
[47] E. Runge, E.K.U. Gross, Phys. Rev. Lett. 52 (1984) 997.
[48] R.E. Stratmann, G. E Scuseria, M. Frisch, J. Chem. Phys. 109 (1998) 8218.
[49] R. Bauernschmitt, R. Ahlrichs, Chem. Phys. Lett. 256 (1996) 454.
[50] M.E. Casida, C. Jamorski, K.C. Casida, D.R. Salahub, J. Chem. Phys. 108 (1998) 4439.
[51] P. Politzer, J.S. Murray, Theor. Chem. Acc. 108 (2002) 134.
[52] L.J. Farrugia, J. Appl. Cryst. 30 (1997) 565.
[53] R.J. Gillespie, J. Chem. Edu. 40 (1963) 295–301.
[54] R.J. Gillespie, Chem. Soc. Rev. 21 (1992) 59–62.
[55] L. Pauling, The Nature of the Chemical Bond, third ed., Cornell University Press, Ithaca, 1960.
[56] J. Bernstein, R.E. Davis, L. Shimoni, N.L. Chang, Angew. Chem. Int. Ed. Engl. 34 (1995) 1555–1573.
[57] V.K. Rastogi, M.A. Palafox, R.P. Tanwar, L. Mittal, Spectrochim. Acta A 58 (2002) 1989.
[58] M. Silverstein, G.C. Basseler, C. Morill, Spectrometric Identification of Organic compounds, Wiley, New York, 1981.
[59] N.B. Colthup, L.H. Daly, S.E. Wiberley, Introduction to Infrared and Raman Spectroscopy, Academic Press, New York, 1990.
[60] G. Socrates, Infrared Characteristic Group Frequencies, Wiley Interscience Publication, 1980.
[61] G. Varsanyi, Vibrational Spectra of Benzene Derivatives, Academic Press, New York, 1969.
[62] G. Varsanyi, Assignments of Vibrational Spectra of Seven Hundred Benzene Derivatives, vol. vols. 1–2, Adam Hilger, 1974.
[63] T. Shimanouchi, Y. Kakiuti, I. Gamo, J. Chem. Phys. 25 (1956) 1245.
[64] D. Sajan, I. Hubert Joe, V.S. Jayakumar, J. Zaleski, J. Mol. Struct. 785 (2006) 43.
[65] D. Michalska, D.C. Bienko, A.J.A. Bienko, Z. Latajka, J. Phys. Chem. 100 (1996) 1186.
[66] G. Socrates, Infrared Characteristic Group Frequencies, Wiley Interscience Publication, New York, 1980.
[67] L.M. Sverdlav, M.A. Kovner, E.P. Krainnov, Vibrational Spectra of Poly Atomic Molecules, Nauka, Moscow, 1970.
[68] L.J. Bellanmy, The Infrared Spectra of Complex Molecules, Chapman and Hall, London, 1980.
[69] P. Vandenabeele, L. Moens, H.G.M. Edwards, R. Dams, J. Raman Spectrosc. 31 (2000) 509.
[70] P.J. Trotter, Appl. Spectrosc. 31 (1977) 30.
[71] D.L. Vein, N.B. Colthup, W.G. Fateley, J.G. Grasselli, The Handbook of Infrared and Raman Characteristic Frequencies of Organic Molecules, Academic Press, New York, 1991.
[72] D. Sajan, I. Hubert Joe, V.S. Jayakumar, J. Raman Spectrosc. 37 (2005) 508.
[73] M. Gussoni, C. Castiglioni, M.N. Ramos, M.C. Rui, G. Zerbi, J. Mol. Struct. 224 (1990) 445.
[74] T.J. Erik Nibbering, T. Elsaesser, Chem. Rev. 104 (2004) 10.
[75] C.H. Wu, A. Ramamoorthy, L.M. Gierasch, S.J. Opella, J. Am. Chem. Soc. 117 (1995) 6148.
[76] A. Ramamoorthy, C.H. Wu, S.J. Opella, J. Am. Chem. Soc. 119 (1997) 10479.
[77] F.A. Cotton, C.W. Wilkinson, Advanced Inorganic Chemistry, third ed., Interscience publisher, New York, 1972.
[78] S.R. Salman, S.H. Shawkat, G.M. Al-Obaidi, Spectrosc. Lett. 22 (1989) 1265.
[79] M. Yıldız, Z. Kılıç, T. Hokelek, J. Mol. Struct. 441 (1998) 1.
[80] H. Nazır, M. Yıldız, H. Yilmaz, M.N. Tahir, D. Ülkü, J. Mol. Struct. 524 (2000) 241.
[81] H. Ünver, M. Yildiz, D.M. Zengin, S. Ozbey, E. Kendi, J. Chem. Crystallogr. 31 (2001) 211.
[82] S.R. Salman, F.S. Kamounah, Spectrosc. Lett. 35 (2002) 327.
[83] M. Yıldız, Spectrosc. Lett. 37 (2004) 367.
[84] H. Tanak, A. Ağar, M. Yavuz, Int. J. Quantum Chem., in press.
[85] Y.X. Sun, Q.L. Hao, W.X. Wei, Z.X. Yu, L.D. Lu, X. Wang, Y.S. Wang, J. Mol. Struct., Theochem 904 (2009) 74.
[86] S.H. Alarcon, D. Pagani, J. Bacigalupo, A.C. Olivieri, J. Mol. Struct. 475 (1999) 233.
[87] B. Chattopadhyay, S. Basu, P. Chakraborty, S.K. Choudhuri, A.K. Mukherjee, M. Mukherjee, J. Mol. Struct. 932 (2009) 90.
[88] Z.C. Rong, L.Z. Jiang, C.Y. Hong, C.H. Shan, Y. Zhi Wu, Y.L. Hua, J. Mol. Struct. (Theochem) 899 (2009) 86.
[89] F.F. Jian, P.S. Zhao, Z.S. Bai, L. Zhang, Struct. Chem. 16 (2005) 635–639.
[90] M. Snehalatha, C. Ravikumar, I. Hubert Joe, N. Sekar, V.S. Jayakumar, Spectrochim. Acta A 72 (2009) 654–662.
[91] Fleming, Frontier Orbitals and Organic Chemical Reactions, Wiley, London, 1976.
[92] T. Karakurt, M. Dinçer, A. Çetin, M. Şekerci, Spectchim. Acta Part A 77 (2010) 189–198.
[93] H. Tanak, M. Yavuz, J. Mol. Mod. 16 (2010) 235–241.
[94] M. Baldini, M. Belicchi-Ferrari, F. Bisceglie, G. Pelosi, S. Pinelli, P. Tarasconi, Inorg. Chem. 42 (2003) 2049–2055.
[95] L.J. Ashfield, A.R. Cowley, J.R. Dilworth, P.S. Donnelly, Inorg. Chem. 43 (2004) 4121–4123.
[96] J.S. Casas, E.E. Castellano, J. Ellena, M.S. Garcia Tasende, A. Sanchez, J. Sordo, M.J. Vidarte, Inorg. Chem. 42 (2003) 2584–2595.
[97] E. Scrocco, J. Tomasi, Adv. Quantum Chem. 11 (1979) 115.
[98] F.J. Luque, J.M. Lopez, M. Orozco, Theor. Chem. Acc. 103 (2000) 343.
[99] P. Politzer, P.R. Laurence, K. Jayasuriya, J. McKinney, Environ. Health Perspect. 61 (1985) 191.
[100] E. Scrocco, J. Tomasi, Topics in Current Chemistry, vol. 7, Springer, Berlin, 1973. p. 95.
[101] C.R. Zhang, H.S. Chen, G.H. Wang, Chem. Res. Chin. U 20 (2004) 640–646.
[102] Y. Sun, X. Chen, L. Sun, X. Guo, W. Lu, Chem. Phys. Lett. 381 (2003) 397–403.
[103] O. Christiansen, J. Gauss, J.F. Stanton, Chem. Phys. Lett. 305 (1999) 147–155.
[104] Z.S. Wang, Y.Y. Huang, C.H. Huang, J. Zheng, H.M. Cheng, S.J. Tian, Synth. Met. 14 (2000) 201–207.
[105] F.L. Huyskens, P.L. Huyskens, A.P. Person, J. Chem. Phys. 108 (1998) 8161.
[106] R. Zhang, B. Du, G. Sun, Y.X. Sun, Spectrochim. Acta A 75 (2010) 1115.
[107] D.W.Y.L. Fei-Fei Li, Polymer 47 (2006) 1749.
[108] K. Oberg, A. Berglund, U. Edlund, B.J. Eliasson, Chem. Inf. Comput. Sci. 41 (2001) 811.
[109] W. Zheng, N.B. Wong, W.K. Li, A. Tian, J. Chem. Theor. Comput. 2 (2006) 808.
[110] A.P. Scott, L. Radom, J. Phys. Chem. 100 (1996) 16502–16513.